LASER VELOCIMETER MEASUREMENT OF REYNOLDS STRESS AND TURBULENCE IN DILUTE POLYMER SOLUTIONS

Thesis by

Samuel Ernest Logan

In Partial Fulfillment of the Requirements

for the Degree of

Doctor of Philosophy

California Institute of Technology

Pasadena, California

1972

(Submitted April 25, 1972)

ACKNOWLEDGEMENTS

The author wishes above all to thank his advisor Professor Hans Liepmann for his encouragement during the author's undergraduate and graduate studies and for patient guidance and support during the experimental program.

The author is also grateful to his father, Mr. Samuel R. Logan, Jr., for services rendered beyond the call of duty in the "bucket brigade" of the polymer measurements.

The author is indebted to the Fannie and John Hertz Foundation for their generous financial support of graduate study and to the Office of Naval Research and Ford Foundation for support of the experimental program.

Finally, the author wishes to thank those who painstakingly labored on this manuscript, the committee of his mother, sister and Mrs. Jacquelyn Beard who did the typing, and Mrs. Betty Wood who prepared the figures.

ABSTRACT

Measurements of Reynolds stress and axial and transverse turbulence intensities have been made in drag-reducing turbulent pipe flow of a dilute solution of high molecular weight polymer and compared to measurements made with pure water. A newly developed laser velocimeter capable of measuring these turbulence parameters has been utilized and is described in detail.

Axial turbulence intensities measured in polymer solution are consistent with previous polymer results and viscous sublayer thickening is observed. New results include demonstration that the turbulent shearing stress is reduced in the turbulent core by an amount proportional to the observed decrease in pressure gradient at the wall, and extrapolates to a wall value in agreement with calculated local wall shear. Near the wall polymer solution Reynolds stress is reduced below that measured for water consistent with observed velocity profiles. Polymer radial turbulence intensities are comparable with those for water in the turbulent core, but exhibit similar dramatic suppression near the wall. These and other recent results strongly suggest that dilute polymer solution drag reduction is primarily a wall phenomenon. Polymers appear to have little or no effect on turbulent flow away from a solid boundary where turbulent velocities scale with u_τ, the shear velocity based on the observed wall shear.

TABLE OF CONTENTS

TABLE OF CONTENTS (cont.)

LIST OF FIGURES

LIST OF FIGURES (cont.)

I. INTRODUCTION

Drag associated with bodies moving through viscous media is of great practical importance and its minimization has long been of considerable interest. Extensive tables have been developed for drag coefficients of various bodies and drag reduction is commonly accomplished by body streamlining. It is well established that ordinary fluids and flow situations exhibit dynamically similar behavior when the parameter UL/ν , the Reynolds number, is the same. This fact, known as Reynolds number similarity, allows universal curves of drag coefficient and friction factor to be determined versus Reynolds number which hold for all ordinary fluids.

A perplexing contradiction to this rule was pointed out by Toms (Ref. 47) in 1948 who noticed that addition of minute amounts of high molecular weight polymer to an ordinary solvent reduced drag or skin friction in turbulent flow significantly more than could be explained by variation in Reynolds number due to small density and viscosity differences. The Toms effect, now well documented, can be dramatic and for certain macromolecules as much as 40 per cent reduction in drag is obtained for as little as 10 parts per million by weight. The phenomenon only occurs in turbulent flows, for selected polymers, and above some "critical shear", dependent on polymer properties.

Thus an alternative method of turbulent drag reduction, by minor modification of the fluid, became apparent and since 1948 the subject has been extensively studied. The comprehensive review of Lumley (1969, Ref. 30) is recommended for detailed background and a brief outline will be presented here.

Only certain macromolecules produce the Toms effect; common examples in water solvent are polyethylene oxide, polyacrylamide, and guar gum. Hoyt and Fabula (Ref. 23) found that the most effective molecules for producing drag reduction had a relatively linear structure with few or no side chains. In addition, Metzner and Park (Ref. 32) found that all drag reducing polymers also exhibit viscoelastic effects in higher concentrations. Viscoelasticity is generally believed to be essential to the Toms phenomenon (Ref. 30) and apparently contributed to some early confusion regarding mechanism as outlined in Gadd (1966, Ref. 15). After several earlier false conclusions (Ref. 14, 16) Gadd concluded that sublayer thickening in drag reducing wall flow was the major effect of polymer additives as concurrently shown by Goren (1966, Ref. 21) and Elata et al. (1966, Ref. 12). Although some qualitative explanations for sublayer thickening and drag reduction have been proposed (Refs. 14, 15, 37, 49, 51), the theoretical basis for the phenomenon is still very poorly established.

In 1967, Wells and Spangler (Ref. 53) conclusively demonstrated that polymer drag reduction is a wall effect by selectively injecting polymer solution into the wall and core regions of a turbulent water pipe flow. In the first case pressure gradient decrease and increased flow were observed; in the second no effect was seen until the polymer diffused to the wall downstream.

Other viscoelastic properties which vary between polymers such as normal stress differences and small eddy suppression in free turbulent flows appear to be secondary phenomena, not intimately related to drag reduction. Degradation, or loss of drag reducing effectiveness (apparently due to chain fracture), occurs under conditions of high shear (Refs. 5, 35). Polymers are subject to degradation in varying amounts: polyox (a polyethylene oxide), the most effective drag reducer (lowest ppm for given reduction) is the most susceptible; separan (a polyacrylamide) and guar gum are both less susceptible, but also somewhat less effective.

Early measurements of turbulence in dilute polymer flow using standard impact or hot wire probes may be somewhat in error due to polymer viscoelastic properties which can introduce extra normal stresses and alter heat transfer characteristics. For these reasons the early measurements of Virk, et al. (1967, Ref. 50) and others, while of great qualitative interest, have been questioned (Refs. 43, 44).

The perturbationless and linear laser velocimeter probe recently developed is a natural alternative and in 1969 was simultaneously utilized by Goldstein et al. (Ref. 17), Chung (Ref. 6), and Rudd (Ref. 42). At present, the best axial measurements and clearest demonstration of sublayer thickening are the recent results of Rudd (1972, Ref. 43) using a laser velocimeter in a square pipe with separan. However, the question of additive effects on other important turbulent parameters such as radial fluctuations and Reynolds stress was left unsettled. Measurement of these quantities would be meaningful in better understanding the mechanisms of turbulent drag reduction by polymer additives and is the intent of this thesis.

A laser velocimeter capable of measuring Reynolds stress and transverse turbulence was recently developed and is utilized in the present experiment. The technique was recently reported (Logan, 1972, Ref. 28) and is described in detail in section III. Rudd's axial measurements are duplicated and confirmed using polyox and extended to include radial fluctuations and Reynolds stress. Preliminary results indicating (in addition to sublayer thickening) the suppression of radial turbulence near the wall and reduction of $\overline{u'v'}$ in the turbulent core proportional to the decrease in wall shear have also been reported (Logan, 1972, Ref. 29). More detailed measurements and results are presented here in sections IV and V.

II. EXPERIMENTAL APPARATUS

2.1 Flow System

A pipe flow was selected for the study of turbulent fluctuations and Reynolds stress in dilute polymer solution for several reasons. Primarily, effects near the wall, which are believed to be of key importance in polymer drag reduction, can be readily studied. Also, relatively small size and flow rate lend themselves to laboratory application, and various concentrations of polymer solution can be easily compared to pure water.

The flow geometry is diagrammed in Figure 1. A 5 gallon constant head reservoir is used to supply a steady flow through the pipe which can be controlled by two valves, one upstream and one downstream of the test section. Potential secondary flows introduced into the pipe flow by elbows before and after the test section are eliminated by honeycomb at each location. A 55 gallon storage reservoir collects the fluid before recirculation to the constant head reservoir. A centrifugal pump is used for recirculating water, whereas for polymer solution the constant head tank was filled manually by bucket to minimize degradation effects. This latter procedure for the polymer solutions was very successful in maintaining steady flow and eliminated severe solution degradation which would result from pumping. (In fact, it was found that 55 gallons of drag reducing polymer solution

was rapidly destroyed when the centrifugal pump was used.)

To allow accurate measurement with the laser velocimeter near the wall the pipe cross sectional area was made as large as possible with the constraint of having only moderate flow rates through the pipe at the highest Reynolds numbers of interest. A maximum allowable flow rate of 10 gallons per minute at Re = 50,000 led to the compromise choice of pipe diameter equal to ½ inch. For ease of measurement near the wall and elimination of test section lens effects which apparently troubled Chung (Ref. 6) in his round tube, a square pipe was constructed, ½ inch on a side, as described in the next section. As indicated in Figure 1, measurements across the pipe were made keeping the optics stationary and positioning the pipe with a micrometer traversing mechanism calibrated to .001".

The total pipe length was $l/d = 70$ with velocity measurements made at $l/d = 65$, to insure fully developed turbulent flow. Wall pressure taps at $l/d = 1, 10, 20, 30, 40, 45, 50, 55, 60, 65, 70$ were used to monitor the pressure gradient along the pipe and determine mean wall shear. The pressure drop was found to be practically linear all along the pipe and in every case the pressure gradient was quite constant being $l/d = 50$ and 70 indicating fully developed flow. (This is shown in Figure 12 which presents pressure drop along the tube for water and polymer.)

2.2 Selection of a Square Pipe

A square pipe was constructed for optical considerations which will be summarized here, although detailed description of the velocimeter will be given in Part III. As diagrammed in Figure 2, the smallest dimension of the focal volume defined by the intersection of the two focused laser beams of the velocimeter is the transverse diameter b_o, which is at least several times smaller than the longitudinal dimension l_o. Thus it is desirable to use the dimension b_o (rather than l_o) as the determining length in velocimeter spatial resolution. This would suggest that (analogous to the use of an oval pilot probe) the long dimension l_o be oriented parallel to a surface in question and the smallest dimension b_o normal to it. However as Chung (Ref. 6) points out, refraction or focusing properties in a round tube practically necessitate orientation of the two intersecting beams in a plane determined by the tube longitudinal axis and a tube diameter to make axial velocity measurements. It is quite evident that this implies use of the distance l_o in a direction normal to the wall which reduces spatial resolution. Obtaining adequate spatial resolution in the very important wall region then requires a larger pipe with correspondingly larger flow rates. It appears that these resolution problems kept Chung from accurately measuring mean velocities and axial turbulence very near the wall in his relatively

small (.468 inch I.D.) round tube.

On the other hand, selection of a square tube does allow the spatial resolution normal to a wall of interest to be determined by the lesser dimension b_o as sketched in Figure 2. As indicated, measurements may easily be made near a wall parallel to the xz plane by merely translating the tube in the y direction. Differential refraction effects characteristic of round test sections upon translating are eliminated. Other velocity components (such as normal to a wall) are similarly easily obtained.

The major drawbacks of a square pipe are loss of symmetry of the round tube and the possibility of secondary flows which can exist in non-circular channels, as first pointed out by Prandtl.(Ref.39) Measurements by Tracy (Ref. 48) in a rectangular channel 5 by 32 inches using air indicated that maximum secondary flows normal to the wall were .0083 U_o where U_o was the centerline velocity. Maximum secondary flows in the ½ inch square pipe were measured to be only about .005 U_o or about 10 percent of the friction velocity $u_\tau = \sqrt{\tau_w / \rho}$ which should not rule out meaningful turbulence measurements. In any case, it is felt that in comparison of water and polymer solutions the square tube should be of no import since relative rather than absolute measurements are of prime concern. Secondary flow effects and measurements are discussed in detail in section 4.3.1 and Appendix D.

III. THE LASER VELOCIMETER

3.1 Introduction

Laser velocimeters have been developed in many research groups across the country in recent years since the concept was first introduced by Yeh and Cummins in 1964 (Ref.54). The basic technique of utilizing the Doppler shift of laser radiation to detect motion of fluids and solids is quite easily applied in laboratory situations as demonstrated in an earlier report (Ref.27).

Measurement of turbulent fluctuations in the streamwise direction by the laser Doppler technique is also well established, having been introduced by Goldstein and Hagan in 1967 (Ref.19) and used by many others in recent years. However, in spite of this developmental work there was for some time no demonstration of laser Doppler measurement of Reynolds stress, $\overline{u'v'}$, or $\overline{v'^2}$, turbulence intensity normal to the mean flow direction. The desirability of measuring Reynolds stress was first mentioned by Goldstein and Hagan but no method was suggested or demonstration given. Direct measurement of turbulence normal to the mean flow direction is not possible with ordinary laser Doppler instruments due to directional ambiguity and low frequency noise.

A simple laser velocimeter capable of turbulence measurements including Reynolds stress and normal fluctuations has been developed and was recently reported (Ref.28). The

background of the laser Doppler technique and the development of this new instrument will be briefly presented.*

3.2 General Background of the Laser Doppler Technique

The theory of the laser Doppler technique and the interpretation of the signals obtained has been extensively given elsewhere (Ref. 36). The basic concept is that light scattered from the common intersection point of two incident coherent beams from the same (laser) source can be mixed in a photodetector to yield a difference (Doppler) frequency which is proportional to the local fluid velocity, $\vec{w}$. As shown in Appendix A, if the two incident beams have initial wavelength λ_o and directions $\hat{e}_1$ and $\hat{e}_2$, the collected radiation will heterodyne with the beat frequency

$$\nu_D = \frac{n\vec{w}}{\lambda_o} \cdot (\hat{e}_1 - \hat{e}_2) \qquad (1)$$

which is the independent of the scattering direction, where n is the index of refraction of the medium. Only one velocity component is measured, lying in the plane of the two intersecting beams and perpendicular to their

---

*Since the submission of Ref. 28 (November 17, 1971) a similar technique for measurement of $\overline{u'v'}$ independently appeared in the literature. (Ref. 10, November 1971).

bisector.* Three common laser Doppler system types in use are the "crossed reference beam" method introduced by Goldstein (Ref. 20) where one beam is used as a local oscillator; the "dual scatter" technique developed by Brayton (Ref. 4), in which only scattered light from both beams is detected; and the "Dopplermeter" developed by Rudd (Ref. 41), which mixes all the scattered and transmitted (unscattered) radiation. These systems are equivalent in principle and each has applications to which it is better suited than the others.

For turbulent flow, it follows from (1) that

$$\overline{\nu_D'^2} = \left(\frac{n}{\lambda_o}\right)^2 \overline{\left(\vec{w}' \cdot (\hat{e}_1 - \hat{e}_2)\right)^2} \qquad (2)$$

where $\vec{w}'$ is the instantaneous vector velocity fluctuation, ν_D' the corresponding instantaneous Doppler frequency fluctuation, and $\overline{\quad}$ indicates time average. (In (2), time averages of fluctuations by definition have been assumed to be zero, $\nu_D' = \vec{w}' = 0$.) Now if θ is the angle

---

*As indicated in Appendix A, the Doppler formula given in equation (1) is actually more general, and also applies to the inverse geometry of light scattered into directions $\hat{e}_1$ and $\hat{e}_2$ from a point illuminated by laser radiation of arbitrary (uniform) direction. Thus, this result may be applied to the early single incident laser beam system of Foreman (Ref. 13) and will be used to explain optical frequency shifting in Part III.

between the intersecting beams, Φ the angle between their plane and the x axis (as depicted in Figure 3) and if $\vec{w}' = u' \hat{e}_x + v' \hat{e}_y$, then (2) becomes

$$\overline{\nu_D'^2} = 4 \left(\frac{n}{\lambda_o}\right)^2 \left[\sin^2\left(\frac{\theta}{2}\right) \overline{u'^2} \cos^2\Phi + 2\overline{u'v'} \cos\Phi \sin\Phi + \overline{v'^2} \sin^2\Phi\right] \tag{3}$$

since $(\hat{e}_1 - \hat{e}_2) \cdot \hat{e}_x = 2\sin(\theta/2) \cos\Phi$, etc.

For the special case of measurement along the x axis, $\Phi = 0^o$ and

$$\overline{\nu_D'^2} = 4 \left(\frac{n}{\lambda_o}\right)^2 \sin^2\left(\frac{\theta}{2}\right) \overline{u'^2} \qquad (\Phi = 0^o) \tag{4}$$

or

$$\sigma_D^2 = \frac{\overline{\nu_D'^2}}{\overline{\nu_D}^2} = \frac{\overline{u'^2}}{\overline{u}^2} \qquad (\Phi = 0^o)$$

by definition of σ^2. The mean flow $\overline{u}$ is found directly from (1) to be

$$\overline{\nu_D} = \frac{2n\overline{u}}{\lambda_o} \sin\frac{\theta}{2} \qquad (\Phi = 0^o) \tag{5}$$

This is the most common (and straightforward) turbulence measurement which has been made in the past where typically $\overline{\nu_D} \gg \overline{(\nu_D'^2)}^{\frac{1}{2}}$. In this case the distribution of ν is a

bell shaped curve about $\overline{\nu_D}$ with width related to $\overline{(\nu_D'^2)}^{\frac{1}{2}*}$. The former gives the mean flow at the point of measurement from equation (5) and the latter the turbulence intensity from equation (4).

However, when the mean flow component in the direction of measurement becomes small or zero, $\overline{\nu_D}$ can become of the order of or smaller than the spectral broadening, and the signal becomes uninterpretable. This situation occurs for example in the measurement of turbulence intensities normal to the flow direction, as in radial turbulence in a pipe, $\overline{v'^2}$, and will be further discussed in section 3.5.

3.3 Instrumental Broadening

For any laser Doppler instrument there is broadening about the mean Doppler frequency $\overline{\nu_D}$ even for steady velocities due primarily to the finite convergence angle $\Delta\theta$ of the two beams and the finite time in which particles cross the focal volume as discussed in Appendix B.3. Experimental investigation verifies that to a good approximation $\Delta\nu_{inst}/\nu \approx \Delta\theta/\theta$, where $\Delta\nu_{inst}$ is the spectral width response to a delta function velocity input. This instrumental broadening must be taken into account when interpreting the turbulent spectra as first noted by Goldstein (Ref. 19). The observed (broadened) spectral width can be easily related to the actual width due only to

*The exact relation between $\overline{\nu_D'^2}$ (and σ_D^2) and the measured spectral width is derived in the next section.

velocity fluctuations by making a reasonable approximation about the shape of the observed spectrum. As pointed out by Goldstein (Ref. 19), the observed spectrum is closely approximated by a Gaussian curve,

$$\frac{I(\nu)}{I_o} = \exp\left(-(\nu-\bar{\nu})^2/2\bar{\nu}^2\sigma^2\right)$$

where I_o is the maximum value observed for mean frequency $\bar{\nu}$. If the width $2\Delta\nu$ is measured at the half maximum, $I(\nu)/I_o = 1/2$, then

$$\sigma^2 = \frac{1}{2\ln 2}\left(\frac{\Delta\nu}{\bar{\nu}}\right)^2 .$$

Now it may be assumed that the instrumental and turbulent velocity distributions are independent random variables so that the observed turbulent variance may be expressed as $\sigma_t^2 = \sigma_D^2 + \sigma_{inst}^2$ and thus

$$\sigma_D^2 = \frac{1}{2\ln 2}\left[\left(\frac{\Delta\nu_t}{\bar{\nu}}\right)^2 - \left(\frac{\Delta\nu_{inst}}{\bar{\nu}}\right)^2\right] \qquad (6)$$

where $2\Delta\nu_t$ is the observed width for turbulent flow (measured at half maximum) and $2\Delta\nu_{inst}$ is the width of the spectrum obtained from a delta function input. Using (6) and (3) the actual turbulent velocity components may be determined from the observed spectral widths since,

by definition, $\sigma_D^2 = \overline{v_D'^2} / \bar{v}^2$.

3.4 Measurement of the Reynolds Stress

It is evident from (3) that the Reynolds stress $\overline{u'v'}$ may be obtained directly from the difference of the variances measured in two perpendicular directions, $\Phi_{1,2} = \pm 45^o$, with respect to the mean flow direction, $\Phi = 0^o$. Using (3), and here defining the variance σ^2 with respect to the maximum velocity in the streamwise (x) direction, U_o :

$$\sigma_{1,2}^2 = \left[\overline{u'^2} + \overline{v'^2} \pm 2\overline{u'v'} \right] / 2U_o^2$$

where use has been made of (5) with $\bar{u} = U_o$.

Thus

$$\sigma_1^2 + \sigma_2^2 = \left[\overline{u'^2} + \overline{v'^2} \right] / U_o^2 \qquad (7)$$

$$\sigma_1^2 - \sigma_2^2 = \overline{2u'v'} / U_o^2 \qquad (8)$$

Quantity (7) is proportional to the total (two dimensional) turbulent energy at the measurement point, while (8) is the local Reynolds stress. Thus, only one receiver is required to measure $\overline{u'v'}$ and simultaneous measurement of u' and v', multiplication, and averaging, is not required. However, the great simplification of only needing one receiver to measure $\overline{u'v'}$ is partly offset by the requirement of having to take two independent measurements ($\pm 45^o$)

at a given point which contributes to increased experimental scatter. A three beam system could be designed to circumvent this drawback such as one recently developed capable of simultaneous measurement of u' and v' (Ref. 3, reported during the preparation of this manuscript.)

Figure 3 illustrates the relationship between the plane of the intersecting beams and the streamwise direction, x. For ease of guaranteeing measurement at the same point in the flow upon rotation (changing Φ) it has been convenient to fix one beam (the reference beam) along the z axis and rotate the other through the desired angle. This will be discussed in more detail with the apparatus in section 3.6.

3.5 Measurement of the Radial Turbulence Intensity

Although the radial turbulence intensity $\overline{v'^2}$ could be inferred through use of equations (4) and (7), direct measurement is preferable. However, merely orienting the intersecting beam plane at $\Phi = 90^{\circ}$ does not allow straightforward measurement of $\overline{v'^2}$ since as mentioned in section 3.2 the mean flow component in that direction, $\bar{v}$, (and thus $\bar{v}_D$) is zero or negligibly small. Fluctuations v' are much larger than $\bar{v}$ so that the spectral distribution becomes centered about zero frequency, and becomes difficult or impossible to separate from the noise spectrum. Low frequency noise exists in the laser beam itself, as

seen in Figure 4. This noise results from reference beam illumination of the photomultiplier tube and resembles a ν^{-1} frequency dependence.

In addition to low frequency noise, laser Doppler systems possess an inherent directional ambiguity due to the square law dependence of the photodetector in the process of heterodyning which allows only the magnitude and not the absolute sense of the Doppler shift to be determined. In general this offers no problem since the flow direction is usually known to within 180^{o}. The solution to this problem (and to the noise problem also) is to introduce a known frequency shift into one of the intersecting beams which is substantially larger than the greatest expected excursion in Doppler frequency. As demonstrated in the next section, the Doppler shift due to the fluid velocity is then added to (or subtracted from) this bias frequency giving absolute directional sensitivity. Frequency biasing also solves the low frequency noise problem, since any given Doppler signal can then be "translated" to center about a predetermined nonzero frequency.

3.5.1 Frequency Offset of the Doppler Signal

As shown in Appendix A, monochromatic radiation of initial frequency ν_o and direction $\hat{e}_1$ scattered into a direction $\hat{e}_s$ from a medium of index n and local velocity

$\vec{w}$ will possess a shifted frequency

$$\nu' = \nu_o \left(1 + \frac{n\vec{w}}{c} \cdot (\hat{e}_s - \hat{e}_1)\right)$$

Now consider radiation from another monochromatic beam of slightly different frequency $(\nu_o + \nu_M)$ and initial direction $\hat{e}_2$ which is simultaneously scattered from the same point into the same direction $\hat{e}_s$. It has the new frequency

$$\nu'' = (\nu_o + \nu_M) \left(1 + \frac{n\vec{w}}{c} \cdot (\hat{e}_s - \hat{e}_2)\right)$$

Heterodyning these two frequencies in a square law detector such as a photomultiplier tube will yield components at the sum and difference of ν' and ν''. Only the difference frequency will be seen since the sum is of order $2\nu_o$, the frequency of light, too fast for photomuliplier response. Thus the current from the photomultiplier will have the fluctuating component

$$\nu_{ac} = \nu'' - \nu' = \nu_M + \left[\nu_o \frac{n\vec{w}}{c} \cdot (\hat{e}_1 - \hat{e}_2)\right] + \left[\nu_M \frac{n\vec{w}}{c} \cdot (\hat{e}_s - \hat{e}_2)\right] \tag{9}$$

The second term of (9) is the Doppler shift of equation (1), ν_D, now biased by a selectable constant frequency ν_M. The last term of (9) is dependent on the scattered direction $\hat{e}_s$ and is non-zero unless $\hat{e}_s$ is chosen in

the direction of $\hat{e}_2$, which amounts to using the frequency shifted beam as the reference beam or local oscillator. However, in general the third term is negligible compared to the first and second terms since $(w/c) \ll 1$ and $\nu_M \ll \nu_o$ respectively. (Typically, both (w/c) and (ν_M/ν_o) are of order 10^{-8} for laboratory applications.)

Thus, to an excellent approximation the Doppler spectrum is frequency shifted by a constant amount ν_M and directional sensitivity is obtained as the Doppler signal ν_D is added or subtracted from ν_M depending upon the fluid direction. (If flow in one direction gives $\nu_M + \nu_D$, flow in the opposite direction (180^o) at the same speed will give $\nu_M - \nu_D$).

The turbulence intensity relations (2) and (3) still hold for the frequency shifted Doppler signal. This has been experimentally verified since no measurable variation in spectral breadth has been observed in the frequency translation of any turbulent spectrum.

3.5.2 Methods of Optical Frequency Shifting

Frequency shifting of laser light can be accomplished in various ways, two of which will be mentioned here. In 1963, Cummins et al. experimentally verified (Ref. 8) the Raman-Nath theory prediction (Ref. 40) that laser light diffracted from ultrasonic waves in water is frequency shifted by an amount equal to the ultrasonic driving frequency times the given diffraction order number. Or, if

the incident laser frequency is ν_o and the ultrasonic wave frequency is ν_M the frequency of a given diffracted order N is

$$\nu = \nu_o + N\,\nu_M \qquad N = 1, 2, \ldots \tag{10}$$

Investigations in an ultrasonic wave cell diagrammed in Figure 5 confirmed this result when various diffracted orders were heterodyned on a photomultiplier tube and displayed on a spectrum analyzer.

Such a frequency shift is easily understood as a Doppler shift introduced into the laser light upon "scattering" from the ultrasonic waves travelling with speed c_s, the speed of sound in the liquid medium. Consider laser light incident normal to the direction of propagation of ultrasonic waves as in Figure 5 and scattered at a small angle ϵ. Then from equation (1), $\vec{w} \cdot (\hat{e}_1 - \hat{e}_2) = c_s \sin\epsilon \cos\epsilon \approx c_s\epsilon$ and the light is frequency shifted to

$$\nu = \nu_o + (n\,\nu_o/c)\,c_s\epsilon \tag{11}$$

For a diffraction maximum N, ϵ must satisfy the diffraction theory relation

$$a\epsilon = N\lambda_o \qquad N = 1, 2, \ldots \tag{12}$$

where $a = c_s/\nu_M$ is the ultrasonic wavelength and λ_o the incident laser wavelength. Result (10) follows immediately

from (11) and (12) using $\lambda_o = c/n\nu_o$.*

Another method of optical frequency shifting employs a "radial diffraction grating" which could be considered a mechanical analog of the ultrasonic diffraction technique. Such a radial diffraction grating, pictured in Figure 6, comes from an optical encoder and was first demonstrated by Stevenson (Ref. 46). Equation (10) still holds, with the modulation frequency $\nu_M = k\omega$ where k is a constant and ω is the angular velocity of the grating. This is easily shown since light scattered in direction ϵ from a point on the grating at radius r has the frequency

$$\nu = \nu_o + \left(n\nu_o/c\right) \omega r \epsilon$$

since ωr is the local speed.

However, now the grating spacing $a = a(r) = 2\pi r/M$ where M is the total number of lines about the grating. Using this and (12) in (13) yields

$$\nu = \nu_o + N\left(\frac{nM}{2\pi}\omega\right)$$

and $k = nM/2\pi$. The important result is that all the light diffracted into a given order has constant frequency independent of r, which makes optical frequency shifting

*An alternate derivation of (10) using the theory of phase modulated waves is given by Adler (Ref. 1).

by radial grating feasible.

The grating was calibrated by heterodyning the zero order (undeflected) beam with a first order beam on a photomultiplier and observing the beat frequency as a function of wheel speed. The resulting frequency shift per order per rpm was 84.2 Hz as shown in Figure 7.

Frequency shifting by ultrasonic waves cannot easily be made less than the low megahertz range (first resonant frequency of a typical piezoelectric crystal), while the radial grating is continuously variable between zero and about .5 MHz (6000 rpm) in the first order with higher frequency shifts available in higher orders. The sub-MHz frequency range is of the order of typical Doppler signals and laboratory electronics, and thus preferred. In addition, incident beam alignment is not critical for the grating, whereas normal incidence is essential for ultrasonic wave diffraction. For these two reasons the radial diffraction grating is utilized in the present laser velocimeter.

3.6 Laser Velocimeter

The laser velocimeter developed and utilized is capable of measurement of mean flow components and turbulence quantities such as $\overline{u'^2}$, $\overline{v'^2}$, and $\overline{u'v'}$ with minimal adjustment of only one optical component, the radial diffraction grating, which serves as a combination

beam splitter, measurement direction selector and frequency modulator. The apparatus is diagrammed in Figure 8. Two of the diffraction orders are selected by a mask and focused in the test section with a single converging lens. This simple arrangement guarantees "self alignment" with the two beams focusing at the same point in the test fluid.* Although there are numerous possibilities such as "dual scatter" it has been convenient to use a "reference mode" system with the zero-order (undeflected) beam serving as a reference beam so that alignment through the fixed lens, apertures and photomultiplier is independent of translation of the grating. Thus measurement at the same point is guaranteed as the measurement direction is changed, for example, from $\Phi = +45^{o}$ to $\Phi = -45^{o}$ in the determination of $\overline{u'v'}$.

Different directions of measurement (various Φ) are selected by translating the diffraction grating parallel to itself, and locating the incident laser beam at different positions around the circumference of the wheel at constant radius, as indicated in Figure 6. Constant radius is important since the line spacing, a , increases linearly with radius. As pointed out in section 3.5, variation in line spacing, a , does not affect the amount of frequency

---

*Focusing and focal volume size for this optical arrangement are discussed in Appendix 3.2.

modulation (for constant grating angular speed) but does change the diffraction angle ϵ (Eq. 12) and therefore velocimeter calibration through changing θ (Appendix B.2).

Most measurements are made with the grating stationary, although by rotating the grating any turbulent spectrum can be shifted in frequency by 84.2 Hz/RPM. As pointed out, this biasing is essential in obtaining $\overline{v'^2}$ ($\Phi = 90^o$) and also useful in bringing other Doppler signals into more convenient frequency ranges. Doppler signals obtained near the wall (with small mean frequencies) are typically frequency shifted into higher ranges to eliminate problems with low frequency noise.

Two spectrum analyzers were used to observe the frequency spectrum of the voltage across the 10-100 kΩ photomultiplier load resistor. The first, a Tektronix 1L5 scope plug in, was used to judge signal quality and general frequency range. The second, a Hewlett-Packard Model 310, slowly scanned the desired frequency range and the output was integrated and recorded on an X-Y plotter.

Figures 9, 10, and 11, taken from Reference 28, demonstrate the capability of the newly developed laser velocimeter technique with water measurements made in the ½ inch square pipe. Axial and radial fluctuations across the pipe are shown in Figure 9. As would be expected on the basis of previous results (Laufer, Ref. 26) the axial

and radial fluctuations approach the same value in the center of the pipe. This suggests the self consistency of the independently measured $(\overline{u'^2})^{\frac{1}{2}}$ and $(\overline{v'^2})^{\frac{1}{2}}$, obtained by somewhat different methods. Figure 10 illustrates turbulent broadening about the biasing frequency ν_M in a typical measurement of $\overline{v'^2}$. (The spectrum with no flow is equivalent to heterodyning the two beams directly together since the scattering occurs from stationary particles in the fluid.) The radial velocity $\bar{v}$, (if non-zero) can be determined by observing a frequency shift in the center of the turbulent spectrum from the constant modulating frequency. Such shifts were observed in the square pipe which indicated secondary flows of order $0.005\ U_o$, as discussed in section 4.3.1.

A typical measurement of the Reynolds stress $\overline{u'v'}$ and two dimensional turbulent energy $\overline{u'^2} + \overline{v'^2}$, is presented in Figure 11. Appendix D shows these measurements of $\overline{u'v'}$, $(\overline{u'^2})^{\frac{1}{2}}$, and $(\overline{v'^2})^{\frac{1}{2}}$ to be mutually consistent in a calculation of the correlation coefficient $k = -\overline{u'v'}/(\overline{u'^2})^{\frac{1}{2}}\ (\overline{v'^2})^{\frac{1}{2}}$, in reasonable agreement with Laufer (Ref. 26).

IV. TURBULENCE MEASUREMENTS IN DILUTE POLYMER SOLUTIONS

4.1 Turbulent Drag Reduction

4.1.1 General Properties

Dilute polymer solutions of Union Carbide Polyox, WSR-301, a single chain polyethylene oxide of average molecular weight of 4×10^6 were prepared as described in Appendix C. Solutions varying between 10 and 100 parts per million (ppm) by weight were used based on previous findings on the effectiveness of polymer additive drag reduction (Ref. 35). Most turbulence measurements were made with the intermediate value of 50 ppm which quite clearly evidenced differences from pure water in drag reduction and turbulent structure.

The most striking evidence of polymer solution drag reduction is the marked decrease in pressure drop along the pipe relative to water at the same Reynolds number. Figure 12 shows representative pressure gradients for water and polymer solutions at two Reynolds numbers measured simultaneously by a multiple water manometer. Drag reduction as much as 69 per cent compared to water was observed at $Re = 54{,}000$ for the 33 ppm polyox solution shown in figure 12(b). Percentage drag reduction, R_D, can be defined as

$$R_D = \frac{(dp/dx)_{water} - (dp/dx)_{polymer}}{(dp/dx)_{water}} \times 100$$

where the water and polymer pressure gradients are determined at the same Reynolds number. R_D was observed to be zero below a critical shear of approximately $(u_\tau)_{crit} = 1$ cm/sec, where $u_\tau = \sqrt{\tau_w/\rho}$ is the shear velocity. The average* wall shear τ_w is determined directly from the pressure gradient dp/dx by $\tau_w = (d/4)(dp/dx)$ where d = pipe diameter (side for a square pipe). Above $(u_\tau)_{crit}$, R_D and drag reduction increase with increasing Reynolds number as shown in Figure 13. For the polymer solution in Figure 13, R_D increases from 40 to 63 percent between Re = 20,000 and 50,000.

The (Darcy) friction factor f is defined as

$$f = \frac{(dp/dx)\, d}{\frac{1}{2}\rho V^2} = \frac{8\tau_w}{\rho V^2}$$

where V is the mean speed computed from the volume flow and tube cross sectional area.** Figure 14 shows f as a function of Reynolds number between 10,000 and 60,000 for

---

*As described in Appendix D, the local wall shear stress can be appreciably greater (or less) than the average wall shear stress as a result of secondary flows in the square pipe. Unless specifically noted to be a local value, τ_w will refer to the average wall shear stress determined from the pressure gradient. Similarly, for consistency, u_τ is calculated from the average wall shear stress τ_w, unless otherwise noted, as in Appendix D.

**The Fanning friction factor, also often called "f", is defined as $f/4$.

water and polymer solution. The water values agree well with Moody's (Ref. 33) measurements in a round pipe, and the drag reducing properties of polymer solution are clearly evident.

4.1.2 Drag Reduction Variation, Degradation, and the Bucket Brigade

Differences in drag reducing properties (R_D, u_τ, etc.) between different batches of polymer solution of the same composition (ppm) appear unavoidable. Even with extreme care in preparation some variations occur between two different batches prepared in the same way (Appendix C). To eliminate experimental scatter resulting from solution variations, each individual velocity profile or turbulence plot utilized only one polymer solution. The pressure drop (and thus u_τ) was monitored continually and noted where appropriate in the Figures.

Polymer degradation, or loss of drag reducing effectiveness, evidently resulting from fracture of the polymer molecules, occurs under the action of shear on the polymer solution and has been studied extensively (Ref. 35). Although a small amount of degradation occurs unavoidably during flow through the pipe system, this effect is kept to a minimum by using a relatively large (200 liters) total volume of polymer solution at one time in a given measurement series. Quite understandably however, it was found

that use of the centrifugal pump rapidly destroyed polymer effectiveness, increasing the pressure drop of the total (200ℓ.) polymer solution of Figure 12(b) to nearly the corresponding pressure drop for water in only 12 minutes at a pump rate of 35 liters/minute. Assuming complete mixing in the supply reservoir, this suggests that total degradation occurred after each molecule had passed through the pump only twice.

Rather than use a more gentle pump (such as the peristaltic pump which Rudd (Ref. 43) found suitable for Separan AP30, but not for polyox) it was decided to transfer all polymer solutions by bucket, keeping the upper constant head reservoir at a constant level during a given measurement. Before the next measurement, several more buckets were filled from the supply reservoir below, transferred above, the valves opened and the process repeated. This "bucket brigade" was found quite satisfactory in supplying a constant flow rate and keeping degradation to a minimum.

4.2 Axial Measurements

4.2.1 Mean Profiles

A comparison between the mean velocity profiles observed for water and 50 ppm polyox solution is given in Figure 15. As observed previously (Refs. 22, 42, 50) the fully developed mean velocity profile for drag reducing polymer flow, compared with water at the same Reynolds number, is flatter (or more "full") in the turbulent core of the pipe flow and less steep near the wall since the wall shear (and thus u_τ) is reduced. Degraded polymer solutions exhibited velocity profiles essentially indistinguishable from profiles measured for water. Figure 16 replots the mean velocity data for water and polymer in terms of the velocity defect law $(U_o - u)/u_\tau$ versus tube position r/R. In the tube center region $(0.2 \leq r/R \leq 1.0)$ polymer solution shows very little difference from water, but considerable difference in slope in the wall region $r/R < 0.2$. As indicated in Figure 16 this result agrees with the results of Goren and Norbury (Ref. 22) who found a similar knee for polymer at $r/R = 0.25$ in their 2 inch pipe. If

$$\frac{U_o - u}{u_\tau} = A \ln(r/R) = B \qquad (13)$$

where A and B are constants, then both water and polymer have the same value for A (and $B = 0$) in the core region but in the wall region the polymer solution assumes a

larger value of A and $B \neq 0$.

These results indicate that polymer flow in the turbulent core closely follows the Newtonian result in the defect law and u_τ , determined by the boundary condition of wall shear stress, is the relevant velocity scale to be used in that region. The effect of the polymer solution near the wall is observed to be a strong function of drag reducing effectiveness, and less effective polymer solutions fell between the results measured for water and the most effective 50 ppm polymer solution plotted in Figure 16.

Figure 17 compares velocity profiles for water and polymer to the universal law of the wall (Coles, 1956, Ref. 7)

$$u^* = \frac{1}{k} \ln y^* + C \qquad (14)$$

where $u^* = u/u_\tau$, $y^* = u_\tau y/\nu$, $k = 0.4$ ("Karman's constant"), and $C = 5.1$. The water measurements are seen to agree favorably with the law of the wall, and the polymer solution beyond the viscous sublayer (linear velocity profile, $y^* \leq 25$) still behaves quite like (14) with a markedly increased value for C and slightly increased slope, or k decreased. Goren (1966, 7, Ref. 21, 22) also found that k was decreased, although Elata (1966, Ref. 12) saw no slope difference from the water curve. The well established displacement of u^* versus y^* results from a thickened viscous sublayer and thus a larger value of y^* where the logrithmic law (14) begins. Velocity measurements

near the wall in the present study confirm this extended linear region as do recent results of Rudd (1972, Ref. 43). Degraded and less effective polymer solutions had values of C approaching those for water, as indicated in Figure 17.

4.2.2 Axial Turbulence Measurements

Axial and transverse turbulence intensities relative to the maximum pipe velocity U_o measured across the pipe for the same Reynolds number are reproduced from Logan (1972, Ref. 29) in Figure 18. All measurements were made at approximately the same U_o (200 cm/sec) and show the general trends that actual turbulence intensities (relative to U_o) are reduced in the core for polymer ($\approx$ .048 compared to .065 for water). However, more proper normalization with respect to u_τ, the relevant velocity scale indicated in the previous section, shows that the axial turbulence intensities are comparable in the pipe center region, $u/u_\tau \approx 1.2 - 1.4$, (Figure 20). In addition, the radial turbulence intensities are seen to agree in magnitude with the axial intensities in the pipe center as expected from previous results (Laufer, Ref. 26) and will be discussed in more detail in section 4.3.2.

Repolotting the axial turbulence intensities near the wall ($0.0 \leq r/R \leq 0.2$) in Figure 19 demonstrates the dramatic sublayer thickening at the same Reynolds number for polymer relative to water. The peak of $(\overline{u'^2})^{\frac{1}{2}}$ is displaced out

from the wall so that near the wall the axial fluctuations are reduced (normalized by U_o, which is the same in both cases) and larger fluctuations are observed for polymer at a greater distance from the wall ($0.05 \leq r/r \leq 0.20$). Although the polymer turbulence intensity is lower in the pipe center, the peak in u' is comparable in magnitude ($(u'/U_o)_{max} \approx 0.20$) with water at the same Reynolds number.

It appears that the sublayer thickening is approximately inversely proportional to the decrease of wall shear stress. For the case illustrated in Figure 19, the sublayer is thickened from r/R of 0.028 to 0.060, a factor of 2.1, while the wall shear, proportional to u_τ^2, fell from 82.8 cm^2/sec^2 to 43.3 cm^2/sec^2, a factor of 1/1.9. An exact relation between sublayer thickening and shear stress reduction could be determined by a series of measurements of this nature.

Figures 20 and 21 present the axial turbulence data of Figure 18 and 19 in terms of u'/u_τ versus r/R and y^* respectively. Figure 20 shows good quantitative agreement in magnitude and behavior with the results of Rudd for a similar square tube (Ref. 43). At the tube center his results vary between 0.8 and 1.3 compared to the present 1.2 - 1.4, whereas for water in $0.1 \leq r/R \leq 0.6$ and polymer $0.1 \leq r/R \leq 0.25$ his intensities are higher. Rudd's peak for water is slightly lower (4.2 compared to 4.8), his peak for polymer higher (8 compared to 6.3). The comparison for

water is regarded as most important, since the polymer result depends on the polymer used (Rudd: separan, Logan: polyox), its concentration (100 ppm, 50 ppm) and the amount of drag reduction obtained (u_τ = 10, 6.6 cm/sec).

For comparison purposes, Laufer in his round tube (Ref. 26) found the values $u'u_\tau \approx 0.8$ in the center and 2.6 at the sublayer peak. However, this is not thought serious since both the higher results obtained here and by Rudd (in agreement with each other) were obtained in square, rather than round, pipes where small secondary flows exist (as discussed in the next section) which may contribute to slightly increased turbulence levels. However, these small secondary flows are not thought to endanger meaningful comparison of turbulence measurements between water and polymer (Rudd, 1969, Ref. 42, and section 4.3.1).*

The axial turbulence intensity is plotted versus y^* in Figure 21 and illustrates again sublayer thickening. The peak in u'/u_τ occurs at $y^* \approx 16$ for water and is delayed for the polymer until $y^* \approx 25$. The water result is in very good agreement with Laufer who also found the u'/u_τ peak at $y^* = 16$ (Ref. 26) and in reasonable

---

*However, as discussed in Appendix D, local secondary flows, although small, can contribute to substantial variations in the local wall shear stress from the average τ_w. Along the plane of measurement, $z = 0$, the local wall shear is significantly larger than the average τ_w. Turbulent fluctuations u' and v' normalized with this larger local shear velocity are closer in magnitude to the measurements of Laufer (Ref. 26).

agreement with Rudd who found the water peak at $y^* = 11$ and the polymer peak at $y^* = 20$. The effect of the polymer is to extend the linear portion of the curve (interpreted as the sublayer) outward to larger values of y^*. Rudd found that the linear portions of the two curves coincided which is nearly but not exactly true in the present results. Coincidence of the linear portions for u'/u_τ versus y^* means that since both solutions obey $u^* = y^*$ in the sublayer the two solutions have the same value of turbulence intensity relative to the local mean flow there. This result suggests, as also pointed out by Rudd (Ref. 43), that only the scale of the sublayer and not the basic structure of the (axial) turbulence is changed.

4.3 Radial Measurements

4.3.1 Radial (Secondary) Flow

As mentioned earlier, small secondary motions resulting from the non circular cross section were measured in the square pipe although these do not appear great enough to adversely affect the comparison between the water and polymer turbulence measurements. L. Prandl, (Ref.39) using a momentum analysis based on the assumption that the turbulence fluctuations tangent to the mean velocity contours are of greater magnitude than those normal to the contours, deduced that secondary motions should be along the bisectors of the corner angle toward the corner and then away from the corner along the adjacent walls. Such motions were reportedly observed by Nikuradse (Ref.34) and an 8 celled secondary flow model for the square pipe based on the theory of Prandtl and Nikuradse is sketched in Figure 22.

More recent work by Eckert and Irvine (Ref.11) in a triangular duct found no indication of secondary motions except when the flow was strongly turbulent. Tracy (Ref.48) measured cellular motion of the Prandtl-Nikuradse type in his rectangular channel and had maximum radial motions normal to the wall of 0.0083 U_o. Rudd (Ref.42) speculated that the secondary flow speeds in his ½ inch pipe were of the order of twenty per cent of the friction velocity u_τ, although he was not able to measure these flows.

The present laser velocimeter is capable of velocity measurement transverse to the main stream by observing small frequency shifts from a constant modulating frequency as previously mentioned in section 3.6 and Fig. 10. Using this method, radial motions normal to a wall and along the bisector of a side, as indicated in Figure 22, were measured in water at Reynolds numbers of 25,000 and 60,000. Along this center plane, motions away from the wall were detected in general, with considerable scatter since the mean velocity frequency shifts were small in comparison with the spectral widths due to velocity fluctuations. (For example, for $Re = 25{,}400$ $v_{s_{max}}/u_\tau = 0.91$ while $(v'^2)^{\frac{1}{2}}/u_\tau \approx 1.5$ at $r/R = 0.2$ from Figure 23.)

In addition, radial velocity measurement is very sensitive to beam plane alignment. Using previous notation (section III) if Φ is not exactly 90° in the radial measurement, say $\Phi = 90^\circ - \epsilon$, then the mean Doppler signal obtained will be $\bar{\nu}_D = (2n/\lambda_o)\sin(\theta/2)[\bar{v} + \epsilon\bar{u}]$. Thus the measured "radial" component will have an additional component $\epsilon\bar{u}$ from the mean flow, which can be substantial even for ϵ small since $\bar{u} >> \bar{v}$. Fine adjustment of the beam plane alignment was made by assuming that mean secondary flow should be zero in the pipe center. Small angular adjustments in Φ were made until the center of the turbulent spectrum of Fig. 10 was identical to the constant modulating frequency ν_M. Thus, the secondary flow

measurements are relative to $\overline{v}$ in the tube center (if non-zero), and small deviations of tube alignment during translation can introduce additional scatter.

The higher Re appears to have a velocity maximum at $r/R \approx 0.1$ and the lower Re a more uniform distribution between 0.1 - 0.4. Apparent flow toward the wall at $r/R \approx 0.7$ may be real if the secondary flow is asymmetric, or may merely be scatter and coincidence.

Detailed secondary flow measurements were not made for polymer solution, although no indications of substantially larger flows than observed for water were seen. Since the maximum secondary flows are only a small fraction of the turbulence fluctuations ($(v_s/v') \approx .09/15 = .06$) their influence on the comparative turbulence measurements should be negligible, although as shown in Appendix D, v_s can cause substantial variation in the local wall shear stress.

4.3.2 Radial Turbulence Measurements

A comparison of radial turbulence measurements across the pipe is given in Figure 23. As mentioned in 4.2.2, in the tube center both water and polymer appear to be essentially isotropic since u'/u_τ and v'/u_τ are nearly equal for both solutions there. In the intermediate region $0.25 \leq r/R \leq 1.0$ both solutions have v'/u_τ constant, and although polymer exhibits slightly lower values than water the distributions of v' appear nearly identical.

However, u'/u_τ in the same region is markedly higher for polymer than for water, which implies that while both solutions show increased anisotropy as the wall is approached (since u'/u_τ becomes significantly larger than v'/u_τ), polymer solution has a greater tendency toward anisotropy than water.

In the wall region, $r/R < 0.25$, polymer solution exhibits markedly decreased values of v' relative to water. For the solutions shown in Figure 23, polymer solution begins to decrease at $r/R \approx 0.2$ while water remains constant until $r/R \approx 0.12$. Expanding the wall region and plotting v'/u_τ versus y^* in Figure 24 shows that in wall coordinates the radial turbulence is suppressed in and beyond the sublayer. Comparison of Figures 24 and 21 shows the relative magnitudes of u' and v' in the wall region for similar solutions of polymer compared to water.

4.4 Reynolds Stress Measurements

Figure 25, (from Logan (1972) Ref. 29), presents a measurement of the Reynolds stress for water and 50 ppm polymer solution at the same Reynolds number of 26,000. Increased scatter compared to previous turbulence measurements of u' and v' results from the fact that the Reynolds stress measurement involves a relatively small difference between two larger numbers, the spectral widths measured at $\pm 45^{o}$. Despite scatter, least squares fits through the two sets of measurements clearly demonstrate that $\overline{u'v'}$ is reduced for polymer solution relative to water. The amount of $\overline{u'v'}$ reduction in the region $0.25 \leq r/R \leq 1.0$ is proportional to the decrease in local wall shear stress for polymer relative to water calculated from the pressure gradient and the secondary motions (Appendix D) as indicated in Figure 25. Linear extrapolations of the $\overline{u'v'}$ curves to the wall are seen to be in good agreement with the calculated local shear values. (As pointed out in Appendix D, the total shear distribution across the tube can vary from strictly linear in the presence of secondary flows, although for Figure 25 linear least squares curves have been fitted through the core measurements).

In comparison to water, polymer solution exhibits marked reduction of $\overline{u'v'}$ in the wall region $r/R < 0.25$.

This effect is a result of the observed velocity profiles for water and polymer solution (Figure 15) and the fact that the total shear τ is the sum of the laminar and turbulent shear stresses, i.e.

$$\tau = \left(\mu \frac{\partial u}{\partial y} - \rho \overline{u'v'}\right) \qquad (15)$$

$$= \tau_w \cdot f(r/R)$$

where τ_w is the wall shear stress, $r/R = 1$ at the pipe center (as previously defined) and $f(0) = 1$ and $f(1) = 0$. For no secondary flow the shear has a linear profile and $f(r/R) = (1 - r/R)$. Thus, since the total shear profile is the sum of the laminar shear and the Reynolds stress, for a given level of total shear, an increased value of $\partial u/\partial y$ at a given radius will result in a lower observed (absolute) value for $-\overline{u'v'}$ there.

As illustrated in Figure 26, the observed Reynolds stress distributions in (c) can be seen to follow from the laminar shear stress $\partial u/\partial y$ in (b) which results from the respective observed velocity profiles (a), as in Figure 15. (The following argument will be made for flow at the same Reynolds number, although an analogous result can be derived for flow for the same wall shear (u_τ) and different Reynolds numbers.)

Under drag reducing conditions at the same Reynolds number (same U_o) the polymer solution mean velocity profile has less slope (smaller $\partial u/\partial y$) than water in both the wall region (i) and the core region (iii). Now since the integral of the slope across the pipe must have the same value for both solutions, i.e.

$$\int_o^R \partial u/\partial y \, dy = U_o \tag{16}$$

it follows that there must be an intermediate region (ii) where $\partial u/\partial y$ is greater for the polymer solution since the integrand of (16) is strictly positive. (The existence of a region (ii) is also obvious from strictly geometric considerations.)

Considering then the total shear stress across the pipe for both cases and using (15) it follows that in region (ii) the Reynolds stress for polymer solution is a smaller percentage of the total stress than in the equivalent water flow. This implies that $\overline{u'v'}$ will be reduced in magnitude farther away from the wall for polymer solution than for water flow, which is the observed effect.

For water and polymer flow at the same wall shear, each solution should have the same total shear distribution across the pipe except near the wall where polymer will exhibit a reduction of $\overline{u'v'}$ relative to water. This results directly from the extended linear region (thickened

sublayer) for drag reducing polymer solution relative to water flow at the same wall shear. Figure 27 compares the polymer measurements of Figure 25 (Re = 26,000 and u_τ = 6.6 cm/sec) with water at the same average wall shear (Re = 14,300 and u_τ = 6.5 cm/sec). The measured values of $\overline{u'v'}$ are normalized by the local wall shear τ_w calculated from the measured pressure gradient and secondary flows. (For the water flow at the lower Reynolds number secondary flow was not measurable, so its effect is neglected and the average wall shear is used in the normalization. For the polymer flow the measured gradient (Figure 16) and secondary flow for water at the same Reynolds number is used in the calculation.)

Near the wall the measured velocity profiles are used to calculate the laminar shear and indicate the expected behavior of the Reynolds stress in the wall region with respect to the linear reference line. The complete shear distribution, which will not be exactly linear, has not been computed in Figure 27.

The measurements of $\overline{u'v'}$ for polymer solution (especially those presented in Figure 27) confirm the previous conclusion that the effect of polymer is primarily near the wall although in a drag reducing situation the proper scaling for $\overline{u'v'}$ in the turbulent core is u_τ^2, which is reduced for polymer relative to water at the same Reynolds number.

V. CONCLUSION

The basic objectives of the thesis programme have been met: to verify the polymer solution axial turbulence measurements of Rudd and extend these measurements to include radial fluctuations and Reynolds stress. To make these measurements, a laser velocimeter with new capabilities was successfully developed and utilized. Detailed thesis results and interpretations have been presented in section IV.

5.1 General Summary of the Results

Measurements are consistent with the generally accepted belief (based previously only on axial measurements) that polymer additives primarily affect the region near the wall and have little effect on the turbulent region far from the wall.

Turbulence measurements presented in this thesis show that the drag reduction phenomenon by certain high molecular weight additives is primarily a wall effect which suggests that free turbulent flows of polymer solution should exhibit negligible differences from comparable water flows. A recent study (Barker, CIT, 1972, private communication) of an axisymmetric jet of polymer into polymer and water into water, using a laser Doppler velocimeter, showed no measurable difference in turbulence intensities or spreading rate between the two flows. This important result is in accord

with the findings of this thesis, and further establishes the importance of the wall in the phenomenon of drag reduction by high molecular weight additives.

From the present pipe flow measurements of mean velocity profile, axial and transverse fluctuations, and Reynolds stress it is evident that the proper velocity scale in the core region $(0.25 < r/R \leq 1.0)$ is u_τ . This indicates that the core flow is largely controlled by the boundary condition τ_w and that polymer additives have little (if any) effect on turbulent structure far from the wall. However, dramatic effects in turbulent structure (axial and transverse fluctuations and Reynolds stress) do occur in the wall region $(r/R < 0.25)$ and polymer additives play a significant role in determining the boundary condition τ_w , which is reduced under drag reducing conditions.

The most evident (and well documented) wall effect is sublayer thickening as observed in the axial mean and fluctuating velocity distributions near the wall. Rudd's (Ref. 43) detailed axial measurements are confirmed, as indicated in section IV. New radial measurements demonstrate that polymer additives also dramatically suppress radial fluctuations near the wall although in the core values of v'/u_τ are comparable to those measured for water.

The measured Reynolds stress, $-\overline{u'v'}$, has been shown to be reduced in the turbulent core by an amount proportional to the reduction in local wall shear τ_w . Computed

values of local wall shear (including secondary flow) are in good agreement with extrapolations of $\overline{u'v'}$ to the wall. In the vicinity of the wall $\overline{u'v'}$ for polymer solution is reduced relative to $\overline{u'v'}$ for water, consistent with requirements of the measured velocity profiles.

The observed reduction in Reynolds stress near the wall is in consonance with earlier estimates of the (completely fictitious) "eddy viscosity", ε , (Refs. 22, 9) which has been shown to be reduced in the wall region. This previous result follows directly from the assumption of a linear total shear distribution and the definition (for the fictitious ε)

$$\tau = \rho (\nu + \varepsilon) \frac{\partial u}{\partial y} \tag{17}$$

Since the velocity profile can be measured and τ_w is clearly reduced, ε is required to decrease in the region near the wall. Goren and Norbury (Ref. 22) found dramatic reductions of ε for polymer solution in the region $r/R < 0.25$. This is in very good qualitative agreement with the present results showing a dramatic reduction of $\overline{u'v'}$ for $r/R < 0.25$ since by "definition", (comparing (17) with (15)), gives

$$\varepsilon = \frac{-\overline{u'v'}}{\partial u/\partial y}$$

The Reynolds stress, $\overline{u'v'}$, and not ε, is real physically. The reduction in ε was deduced in earlier investigations from the velocity profile and (17), whereas here $\overline{u'v'}$ was measured independently and found to be in agreement with the measured velocity profile (section 4.4).

Of qualitative interest here is the work of Phillips (Ref. 38) who derives a result for the gradient of the Reynolds stress in terms of the second derivative of the

$$\frac{d(\overline{u'v'})}{dy} = A\theta\,\overline{v'^2}\,\frac{d^2u}{dy^2} \qquad (18)$$

velocity profile $u(y)$, where A is a constant, and θ is the convected integral time scale of the v' fluctuations. According to this model the Reynolds stress gradient (and not $\overline{u'v'}$) is a "local" property, and depends on the kinetic energy density of the vertical velocity fluctuations, $\overline{v'^2}$. For pipe flow Phillips shows that the (fictitious) "eddy viscosity" may be expressed as

$$\varepsilon = A\theta\,\overline{v'^2}$$

Thus, according to the model of Phillips, the measured reductions in both $\overline{u'v'}$ and $\overline{v'^2}$ in the wall region are mutually consistent.

5.2 Previous Speculation on Drag Reduction Mechanism

There have been various speculations put forward attempting to explain this mechanism of high molecular weight polymer drag reduction, although the question still remains unanswered. Several of these speculations will be briefly mentioned although it must be emphasized that further extensive investigations are needed in order to establish if any of these proposals have factual basis.

The most well-known proposals seem to be those by Pfenninger (Ref. 37), Gadd (Refs. 14, 15) and Tulin (Ref. 49) all qualitatively suggesting how polymer additives primarily affect the wall region, thickening the viscous sublayer and reducing turbulent skin friction. Pfenninger's hypothesis is based on observations and speculation by Kline (Refs. 24, 25) and others that longitudinal eddies formed near the wall are involved in the generation of turbulence as they are stretched and convected away from the wall, "bursting" at some critical Reynolds number.

Kline et al. (Ref. 25) have suggested (from water observations) that this bursting process contributes to instantaneously large values of $-u'v'$ and hence streak breakup makes a substantial contribution to the turbulence energy production per unit volume in the wall region. If polymer additives somehow inhibit this bursting (as speculated by Pfenninger and Gadd (Ref. 15)) then locally

reduced values of $\overline{u'v'}$ should result near the wall for drag reducing polymer solution. This is a possible explanation for the observed reduction in $\overline{u'v'}$ near the wall for polymer solution, although extensive further investigations are required to establish the real mechanism of drag reduction.

Gadd's speculation (Refs. 14, 15) further suggests that longitudinal polymer molecular alignment and viscoelastic effects should suppress turbulent motions transverse to this alignment. The observed suppression of $\overline{v'^2}$ near the wall by polymer additives is in accord with this speculation, but in itself is not sufficient to test Gadd's hypothesis.

Alternative models by Tulin (Ref. 49) and Walsh (Ref. 51) each postulate mechanisms for drag reduction based on energy considerations, although neither can a priori predict the phenomenon.

5.3 Suggestions for Further Work

Extension of the present investigation to a flow situation such as a round pipe which would not exhibit secondary flow would be desirable. Although the square pipe is very advantageous optically, the inevitable secondary flows cause undesirable effects such as wall shear stress variations and possibly increased turbulence levels.

Detailed spectral analysis of u' and v' should be made in the wall region to determine which scales of turbulence are most affected by polymer additives. This, as well as detailed visual observations on polymer wall flows analogous to those of Kline (Ref. 25) would give a firmer basis on which to establish a theory for drag reduction by high molecular weight polymer additives. Extension to the case of flow over rough walls would also be of interest.

APPENDIX A. DOPPLER FORMULA DERIVATION

The laser Doppler formula (1) can be quite easily derived by considering a particle moving with velocity $\vec{w}$ and irradiated with monochromatic radiation of frequency ν_o in direction $\hat{e}_o$. Neglecting relativistic effects, the particle will view (and scatter) this radiation in its

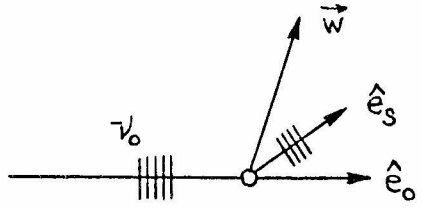

moving frame at the shifted frequency

$$\nu_p = \nu_o \left(1 - n\hat{e}_o \cdot \frac{\vec{w}}{c}\right)$$

where c/n is the local speed of light. Light scattered into a direction $\hat{e}_s$ when viewed in the laboratory (transmitter) frame will have the frequency

$$\nu_s = \nu_p \left(1 + n\hat{e}_s \cdot \frac{\vec{w}}{c}\right)$$

so that the light has received a total frequency shift of

$$\Delta\nu = \nu_s - \nu_o = \nu_o \frac{n\vec{w}}{c} \cdot (\hat{e}_s - \hat{e}_o) \qquad (A.1)$$

neglecting terms of order $(w/c)^2$. The magnitude of $\Delta\nu$ is of the order (or less than) 10^6 Hz since $\nu_o = O(10^{14}$ Hz), $(w/c) = O(10^{-8})$ and the dot product varies between zero

and one. Equation (A.1) also shows the linear and unidirectional response of the Doppler frequency shift.

The dependence of the observed Doppler shift on the scattered direction $\hat{e}_s$ can be eliminated by considering simultaneous illumination of the scattering particle by two incident monochromatic beams of frequency ν_o and respective directions $\hat{e}_1$ and $\hat{e}_2$.

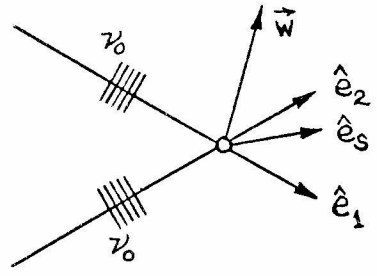

Light scattered by the first beam into an arbitrary direction $\hat{e}_s$ will have the frequency

$$\nu_{s_1} = \nu_o \left(1 + \frac{n\vec{w}}{c} \cdot (\hat{e}_s - \hat{e}_1)\right)$$

Light scattered by the second beam into the same direction $\hat{e}_s$ will have the frequency

$$\nu_{s_2} = \nu_o \left(1 + \frac{n\vec{w}}{c} \cdot (\hat{e}_s - \hat{e}_2)\right)$$

Heterodyning (mixing) these two in a nonlinear detector will yield the sum and difference frequencies $(\nu_{s_1} + \nu_{s_2})$ and $(\nu_{s_1} - \nu_{s_2})$. But since the photomultiplier detector acts like a low pass filter and averages out the sum frequency

($O(10^{14}$Hz)) only the difference frequency will be detected in the anode current, or

$$\Delta\nu = \nu_{s_1} - \nu_{s_2} = \nu_o \frac{n\vec{w}}{c} \cdot (\hat{e}_2 - \hat{e}_1) \qquad (A.2)$$

which is <u>independent</u> of the scattering direction $\hat{e}_s$.

Equation (A.2) can be easily shown to also apply to the case of two scattered beams from a particle illuminated by an incident beam of arbitrary direction. Extension of the Doppler formula to multiple particle scattering from a finite sized focal volume (Appendix B.2) has been treated by Wang, Ref. 52.

APPENDIX B. LASER VELOCIMETER OPTICAL CONSIDERATIONS

B.1 Selection of Beam Angle θ

The choice of θ involves compromise. Primarily θ is selected so that ν_D (which is proportional to $\sin(\theta/2)$) is within a desired frequency range, usually in the sub- or low MHz range for low speed laboratory applications. Within this constraint, larger θ gives smaller focal volumes (Appendix B.2) although slightly less scattered light in the reference beam direction since Mie scattering peaks very strongly in the forward direction, small θ (Ref. 13). For the present experiments θ varied between 5^o and 10^o which kept ν_D usually less than 500 kHz.

B.2 Focal Volume Size

For adequate spatial resolution near the wall where velocity gradients are large the focal volume should be as small as possible. For the conventional self-aligning laser velocimeter which uses two parallel beams focused by a single converging lens the focal volume has the diameter b_o (which defines the resolution in the direction normal to the

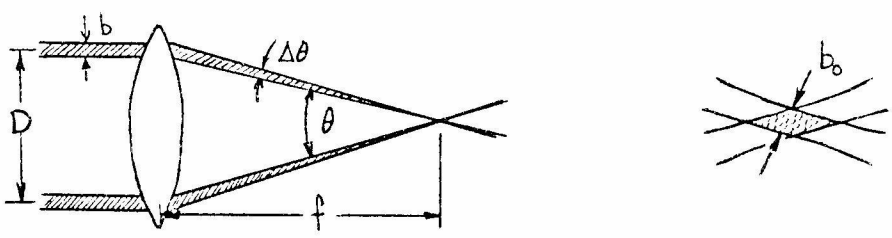

beam plane) where $b_o = (4/\pi)(f/b)\lambda$, (Ref. 4). For typical values ($\lambda = .633\mu$, f = 10 cm., b = 1 mm.) $b_o = 0.08$ mm. It

is seen that either large values of b (as Rudd employed) or small values of f (usually associated with large θ) will decrease b_o and improve spatial resolution in that direction. A comprehensive discussion of spatial resolution, accuracy, and system design is given by Brayton (Ref. 4).

A slightly larger focal volume results for the laser velocimeter utilizing the radial diffraction grating in Figure 8. The (exaggerated) illustration depicts the displaced

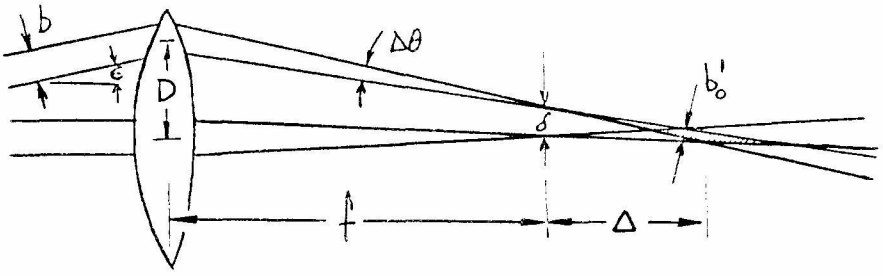

(by Δ) focal volume with broadened diameter b_o' resulting from the (small) angle ε. Using the simple lens formula it is straightforward to show that $\delta \approx f$ and $\Delta \approx (\varepsilon f^2)/D$. Estimating $b_o' \approx (\Delta\theta)\Delta$ gives $b_o' \approx \varepsilon f(b/D)$. For the system of Figure 8, $\varepsilon = 0.014$ and again using f = 10 cm., b = 1 mm., and (b/D) = 0.1 gives $b_o' \approx 0.14$ mm. and $\Delta \approx 1.4$ cm. Thus although the focal volume displacement Δ can be large, the focal volume diameter can remain small if f and (b/D) are both kept minimal.

B.3 Instrumental Broadening of the Doppler Spectrum

The instrumental broadening $\Delta\nu_{inst}$ used in equation (6) is determined from the Doppler spectral width obtained from a delta function velocity input, a lucite wheel rotating at

constant speed. For the present system $\Delta \nu_{inst}/\nu \approx 0.1$, the same order as $(b/D) = (\Delta\theta/\theta)$. This is easily seen in either of two ways, either from the finite convergence angle $\Delta\theta$ and the Doppler formula, or from the finite number of fringes N in the focal volume (using the "fringe model" of Rudd (Ref. 41)). The first, since the Doppler formula can be written as $\nu_D = (2nv/\lambda_o)\sin(\theta/2)$, yields $\Delta\nu/\nu = \frac{1}{2}\cot(\theta/2)\Delta\theta \approx \Delta\theta/\theta$ for small θ.

The alternative derivation for broadening based on the fringe model gives the same result. Each particle in passing through the focal volume generates N cycles and thus has a frequency uncertainty proportional to 1/N. The fringe

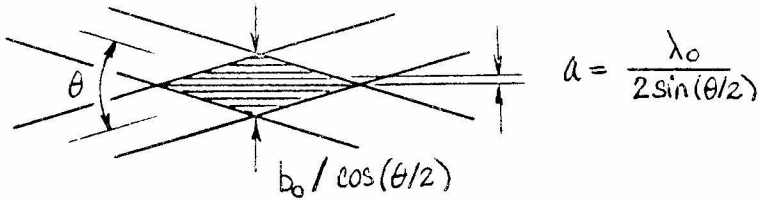

spacing, a, can be shown to be $a = \lambda_o/(2\sin(\theta/2))$ and since the transverse dimension is $b_o/\cos(\theta/2)$, the total number of fringes is

$$N = \frac{b_o}{\cos(\theta/2)} \cdot \frac{2\sin(\theta/2)}{\lambda_o}$$

$$= \frac{8}{\pi} \frac{f}{b} \tan(\theta/2)$$

Now since $(b/f) = \Delta\theta$,

$$1/N = (\pi/8)\cot(\theta/2)$$

$$\approx (\pi/4)\cdot(\Delta\theta/\theta) \quad \text{for small } \theta.$$

APPENDIX C. POLYMER SOLUTION PREPARATION

The polymer solution is prepared in a manner shown previously to be successful (Ref. 2). A (20 liter) master solution of 10 times the final concentration is first prepared and thoroughly mixed before dilution to the total (200 liter) volume used in a given test. The master solution is prepared by thinly and evenly sprinkling polyox powder over the surface of 20 liters of solvent being slowly stirred by a 60 RPM paddle. The powder is allowed to go into solution before more powder is sprinkled over the surface. In this manner the entire amount of polymer (2 grams for 10 ppm, 20 grams for 100 ppm) can be dissolved in several hours and lumps avoided. After several additional hours of stirring, the master solution is allowed to stand overnight and diluted to 200 liters the following day. The final solution is then mixed by 60 RPM paddle for several hours before being used.

APPENDIX D

DISCUSSION OF WALL SHEAR DETERMINATION AND MAGNITUDE OF THE MEASURED REYNOLDS STRESS

The wall shear τ_w (and thus the friction velocity $u_\tau = \sqrt{\tau_w/\rho}$) can be determined in three ways: from the tube pressure gradient, the wall velocity gradient, and from the measured Reynolds stress. As pointed out in the text the tube pressure gradient which defines the <u>average</u> wall shear was used to compute the shear velocity u_τ in every case.

A simple momentum balance for (constant area) pipe flow gives for the average wall shear

$$\left(\tau_w\right)_{av.} = \left(\frac{A}{S}\right)\frac{dp}{dx} \qquad (D.1)$$

where A is the cross sectional area, and S is the surface area per unit length (or circumference). For either a round or square pipe, both of diameter d $(=2R)$, result (D.1) becomes

$$\left(\tau_w\right)_{av.} = \left(\frac{d}{4}\right)\frac{dp}{dx} \qquad (D.2)$$

Since the pressure gradient was continuously measured for every run, this was the most consistent way to define the

shear velocity u_τ .

The local wall shear can be determined from the other two methods mentioned. In the second by definition

$$\left(\tau_w\right)_{local} = \mu \left(\frac{\partial u}{\partial y}\right)_o \qquad (D.3)$$

where o refers to the measured velocity gradient at the wall. This method was not used since the wall gradient was not measured in every case and is also strongly dependent on focal volume size. It was found experimentally that larger focal volumes gave measured velocity gradients near the wall smaller than those expected from the measured pressure gradient. (Better agreement was obtained with the pressure gradient result when the focal volume was made sufficiently small, although values still tended to be low.) Goldstein and Adrian (Ref. 18) derive two alternative methods of determining velocity gradients near the wall assuming finite focal volume size, although these are not used here.

A third determination of local τ_w is possible from an extrapolation of measured $\overline{u'v'}$ in the core region to the wall assuming a linear distribution for the total shear. This method suffers from the assumption of a linear total shear across the pipe (shown invalid with secondary flows in the next section) and the large scatter inherent

in the $\overline{u'v'}$ measurements. Linear extrapolation of $\overline{u'v'}$ to the wall should give a value of wall shear in agreement with the average wall shear computed from the pressure gradient, ρu_τ^2 . Reasonable agreement was obtained for lower speed flows (as Re = 14,300 in Figure 27), although higher speed flows (Re = 26,000 and 60,000) gave values consistently higher than average in this extrapolation. Measurements at these higher two Reynolds numbers are presented in Figure D.1 normalized with the computed average wall shear stress (R/2) (dp/dx) and show indicated local shear of up to nearly twice the average in some cases. This result, which caused much early concern, has been shown to result from local wall shear variation due to secondary flows. Lower speed turbulent flows, exhibiting insignificant secondary motions, should have less wall shear variation and thus better agreement between average and local values. This was observed to be the case.

It is at first quite surprising that the existence of small secondary flows can greatly alter the total shear stress distribution from linear and cause significant deviations of local wall shear from the average. For pipe flow with a non-zero mean radial velocity v the (time averaged) equation of motion is

$$\rho v \frac{\partial u}{\partial r} = - \frac{\partial p}{\partial x} + \frac{1}{r} \frac{\partial}{\partial r} (r\tau)$$

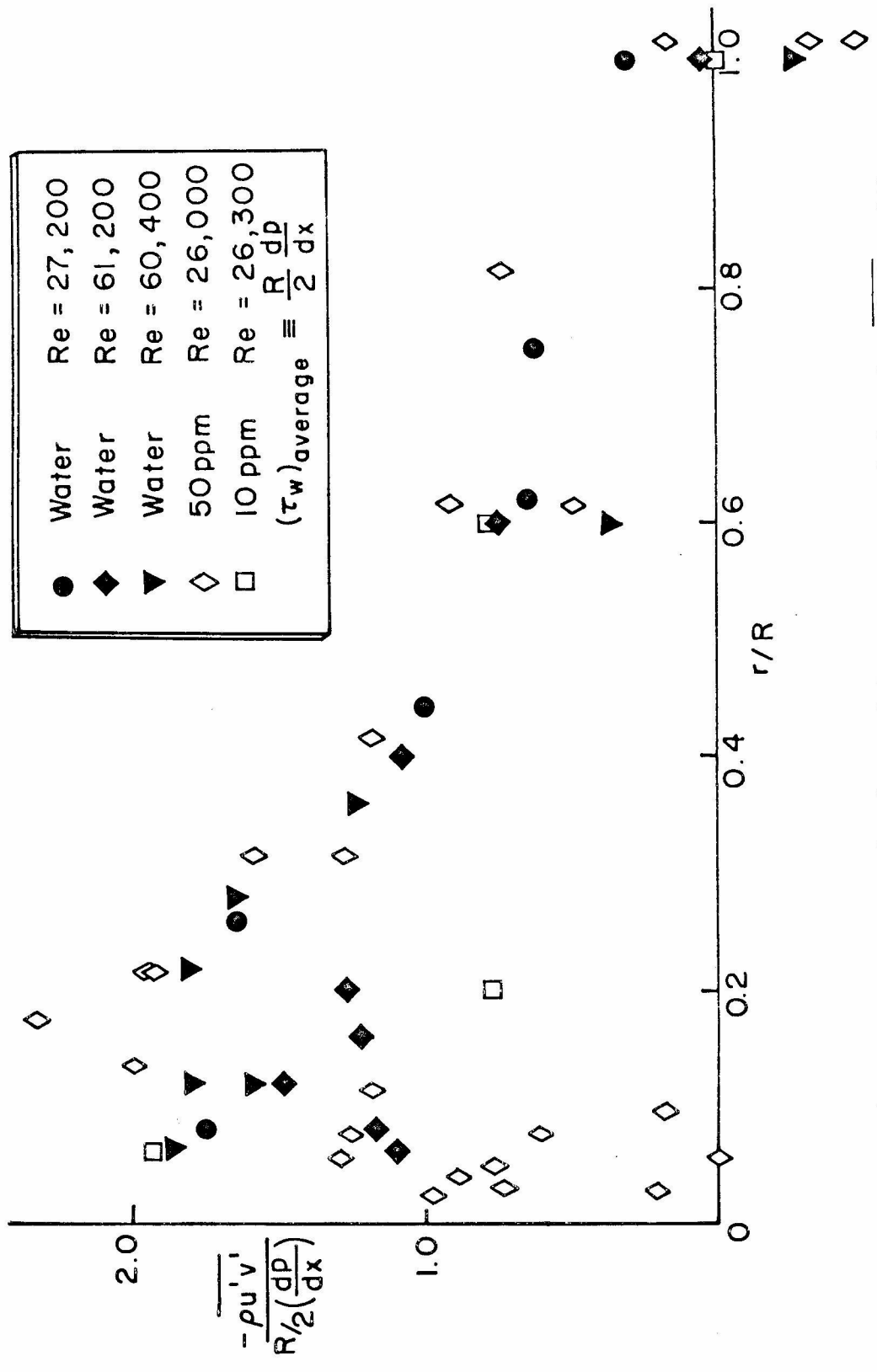

Figure D.1 Correlation of laser-measured local $\overline{u'v'}$ with the average wall shear computed from dp/dx for higher Reynolds numbers where secondary flows are significant.

where u, v, p, τ are mean values, and $\tau = \mu \frac{\partial u}{\partial r} - \rho\overline{u'v'}$. Integrating gives

$$\tau(r) = \left(\frac{\partial p}{\partial x}\right) \frac{(R-r)}{2} + \frac{\rho}{r} \int_{r}^{R} v \frac{\partial u}{\partial r} \, r dr \qquad (D.4)$$

where $r = 0$ is the pipe wall and $r = R$ the pipe center as previously defined. When $v = 0$ the standard linear distribution results for $\tau(r)$ and $\tau_w = (R/2)(\partial p/\partial x)$ as before (Eq. D.3). When $v \neq 0$ the integral in (D.4) can contribute significantly to $\tau(r)$ which is then no longer linear. Calculations using measured secondary flows for water (Fig. 22) and measured velocity gradients (Fig.16) indicate that this effect can be important when non-zero radial velocities exist in regions of large velocity gradients near the wall. Figure D.2 shows the results of calculations for the two highest Reynolds numbers in water for which significant secondary motions were detected (Figure 22). Near the center of the pipe, $0.5 < r/R < 1.0$, deviations from linear are small since velocity gradients are small there. However, near the wall where $\partial u/\partial y$ is large the total shear can increase to 1.8 to 1.9 to the average wall shear determined from the pressure gradient, $(R/2)(\partial p/\partial x)$. The large magnitude of the effect was very surprising since the secondary flow v is only 10 percent of the friction velocity u_τ. (In other parts of the pipe where secondary flows are of opposite direction the local

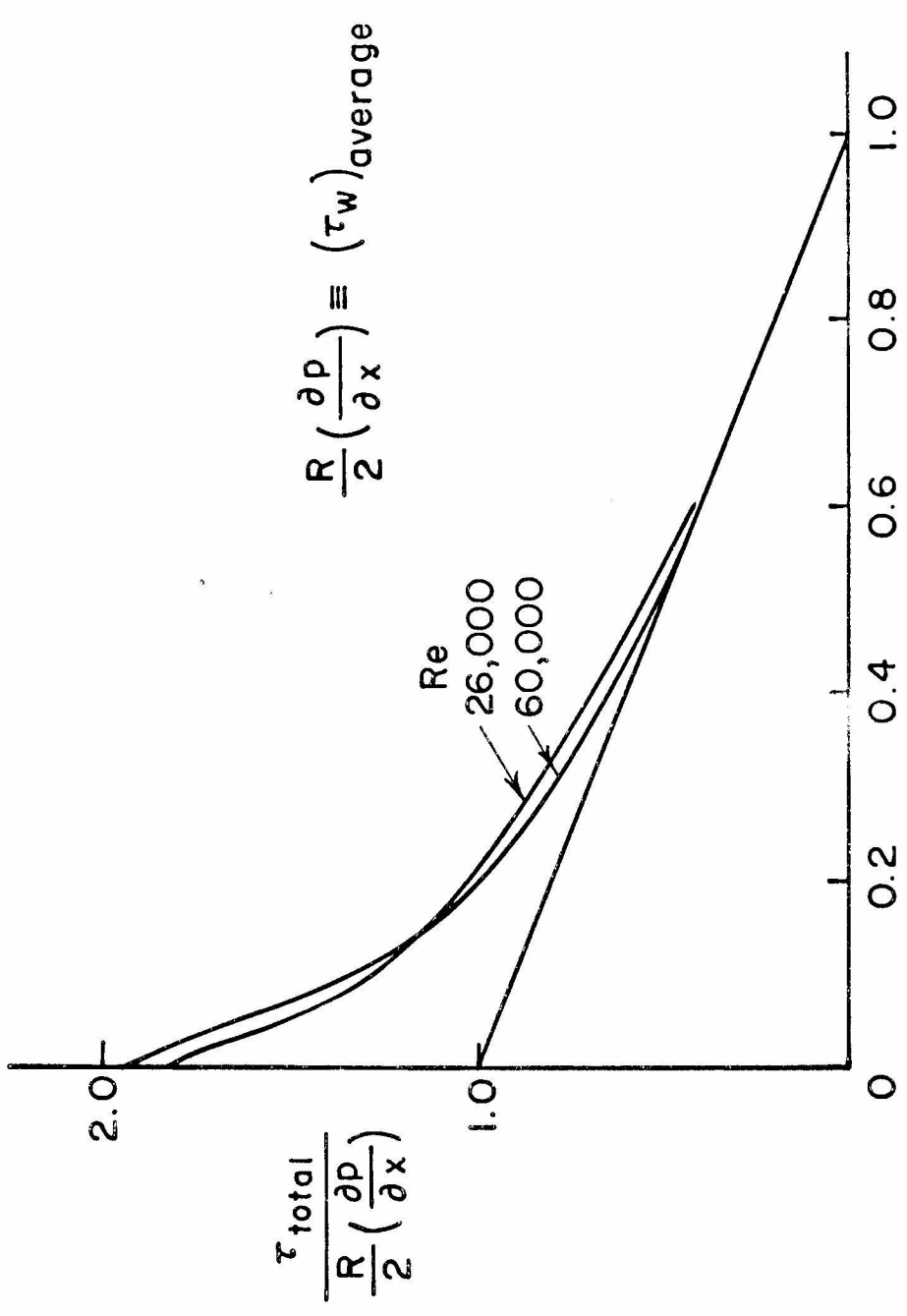

Figure D.2. Effect of secondary flow on total (local) shear stress

shear will be reduced relative to the average.)

The computational method was used to determine the local wall shear in Figure 25, in good agreement with the extrapolated $\overline{u'v'}$ measurements, which lends confidence to both the $\overline{u'v'}$ measurements and the explanation of wall shear variation due to secondary flow. Earlier questions of possible systematic error or broadening of the $\overline{u'v'}$ measurements were discarded (after careful checking) for several reasons. First, all Reynolds stress determinations were consistently computed from equations (8) and (6) which are in agreement with previous derivations. Secondly, the axial turbulence measurements are in agreement with Rudd (Refs. 42, 43) who used a laser velocimeter in an identical square pipe, which lends credence to the radial and Reynolds stress measurements computed in similar manner. In addition, the relative magnitudes of $(\overline{u'^2})^{\frac{1}{2}}$, $(\overline{v'^2})^{\frac{1}{2}}$, and $\overline{u'v'}$ are in consonance as seen in a computation of the correlation coefficient $k = \overline{u'v'}/(\overline{u'^2})^{\frac{1}{2}}\ (\overline{v'^2})^{\frac{1}{2}}$ which is of the order of 0.40 $(r/R \approx 0.3)$ for both water and polymer as shown in Figure D.3. This is in reasonable agreement with Laufer's results for a round pipe (Ref. 26) and indicates that the three measurements are consistent in magnitude among themselves.

Since for the strongest turbulent flows the correct local value for u_τ can be as much as 1.3 to 1.5 times larger than the average, computations of u'/u_τ and

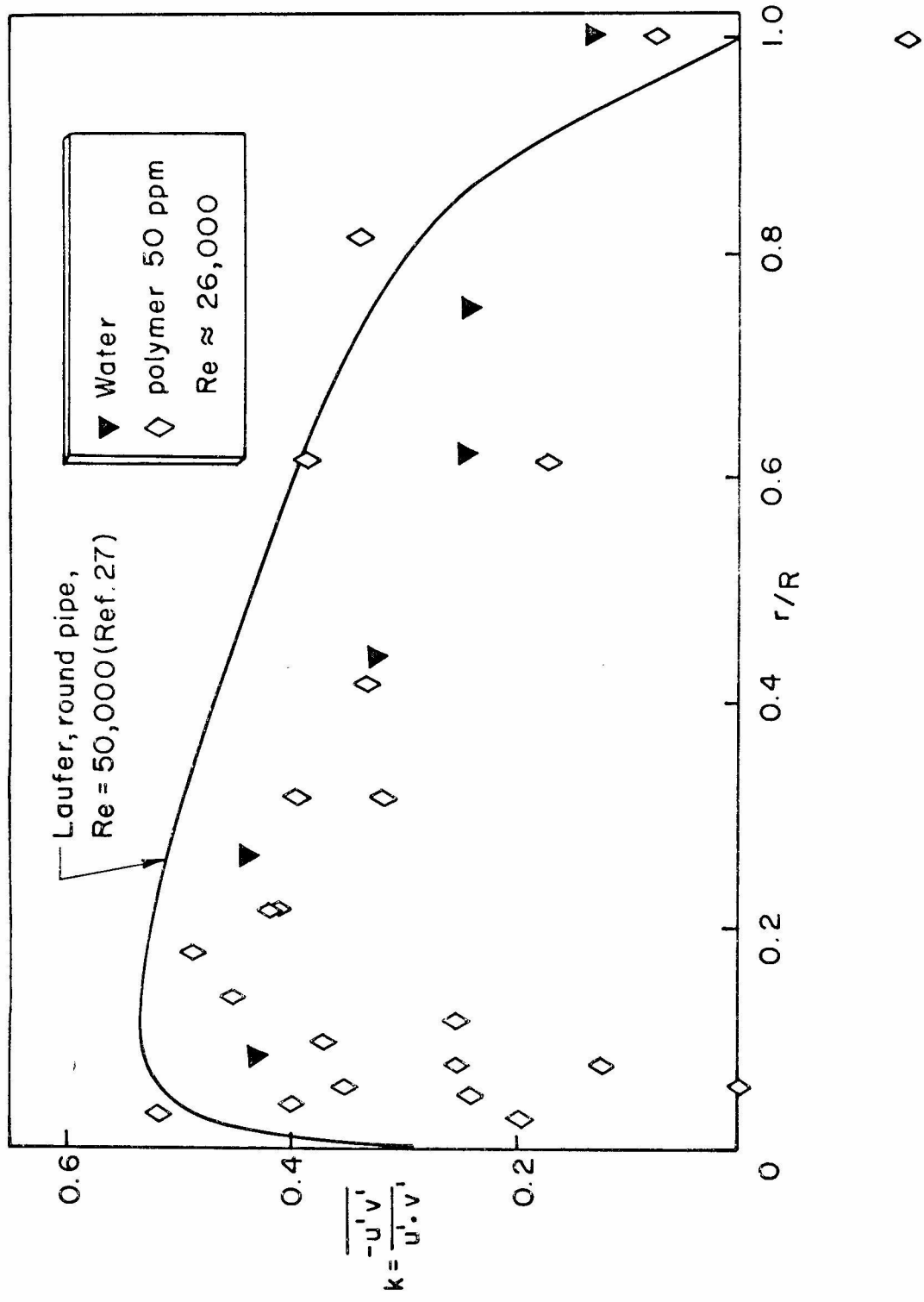

Figure D.3 Comparison of correlation coefficient, k , across pipe for water and polymer

v'/u_τ using this local value will be significantly smaller and in much better agreement with the magnitudes measured by Laufer. However, normalizations with the average u_τ are consistent and exhibit the essential comparisons between water and polymer that were sought. The investigations of Rudd, performed in a similar square pipe, should be similarly affected by secondary flow and local shear variation, although he did not measure the radial motions or $\overline{u'v'}$ in his experiment.

REFERENCES

1. Adler, R., "Interaction Between Light and Sound," IEEE Spectrum, 4, 42, (May, 1967).

2. Barker, S. J., "Radiated Noise and Wall Pressure Measurements in Turbulent Boundary Layers in Dilute Polymer Solutions," PhD thesis, California Institute of Technology, (1971).

3. Bourke, P. J., Brown, C. G., and Drain, L. E., "Measurement of Reynolds Shear Stress in Water by Laser Anemometry," Disa Information, 12, 11, (November 1971).

4. Brayton, D. B., "A Simple Laser, Doppler Shift, Velocity Meter with Self Aligning Optics," Electro-Optical Systems Design Conference, (September 16-18, 1969), New York Colliseum.

5. Brennan, C.,and Gadd, G. E., "Aging and Degradation in Dilute Polymer Solutions," Nature, 215, 1368, (1967).

6. Chung, J. S., "Laser Anemometer Measurements of Turbulence in Non-Newtonian Pipe Flows," PhD thesis, University of Michigan, (1969).

7. Coles, D., "Law of the Wake in the Turbulent Boundary Layer," J. Fluid Mech., 1, (1956).

8. Cummins, H., Knable, N., Gampel, L., and Yeh, Y., "Frequency Shifts in Light Diffracted by Ultrasonic Waves in Liquid Media," Applied Physics Letters, 2, No. 3, 62, (1963).

9. Debrule, Paul M., "Friction and Heat Transfer Coefficients in Smooth and Rough Pipes with Dilute Polymer Solutions," PhD thesis, California Institute of Technology, (1972).

10. Durst, F. and Whitelaw, J. H., "Measurements of Mean Velocity, Fluctuating Velocity, and Shear Stress in Air Using a Single Channel Optical Anemometer," Disa Information, 12, 11, (November, 1971).

11. Eckert, E. G. R., and Irvine, T. F., "Flows in Corners of Passages with Non-Circular Sections," Transactions, ASME, 78, 709, (1956).

REFERENCES (cont.)

12. Elata, E., Lehrer, J., and Kahanovitz, A., "Turbulent Shear Flow of Polymer Solutions," Israel Journal of Tech., 4, 87, (1966).

13. Foreman, J. W., et. al., "Fluid Flow Measurements With a Laser Doppler Velocimeter," IEEE J. Quant. Elect., 2, No. 8, 260, (1966).

14. Gadd, G. E., "Turbulence Damping and Drag Reduction Produced by Certain Additives in Water," Nature, 205, 463, (1965).

15. Gadd, G. E., "Reduction of Turbulent Friction in Liquids by Dissolved Additives," Nature, 212, 874, (1966).

16. Gadd, G. E., "Differences in Normal Stress in Aqueous Solutions of Turbulent Drag Reducing Additives," Naure, 212, 1348, (1966).

17. Goldstein, R. J., Adrian, R. J., and Kreid, D. K., "Turbulent and Transition Pipe Flow of Dilute Aqueous Polymer Solutions," I & EC Fund., 8, No. 3, 498,(1969).

18. Goldstein, R. J., and Adrian, R. J., "Measurement of Fluid Velocity Gradients Using Laser-Doppler Techniques," Rev. of Sci. Inst., 42, No. 9, 1317, (1971).

19. Goldstein, R. J., and Hagan, W. F., "Turbulent Flow Measurements Utilizing the Doppler Shift of Scattered Laser Radiation," Physics of Fluids, 10, 1349, (1967).

20. Goldstein, R. J., and Kreid, D. K., "Measurement of Laminar Flow Development in a Square Duct Using a Laser-Doppler Flowmeter," Journal of Applied Mechanics, 34, E, 813, (1967).

21. Goren, Y., PhD thesis, Department of Mechanical Engineering," University of Liverpool, England, (1966).

22. Goren, Y., and Norbury, J. F., "Turbulent Flow of Dilute Aqueous Polymer Solutions," Transactions of the ASME, Journal of Basic Engineering, Paper No. 67-WA/FE-3, (1967).

REFERENCES (cont.)

23. Hoyt, J. W., and Fabula, A. G.,"Effects of Additives on Fluid Friction," Proc. of the Fifth Symposium on Naval Hydrodynamics, Bergen, Norway, 947, (1964), (ACR-112, ONR, Wash. D. C.).

24. Kline, S. J., and Runstadler, P. W., "Some Preliminary Results of Visual Studies on the Flow Model of the Wall Layers of the Turbulent Boundary Layer," Stanford University Report MD-3, (1958).

25. Kline, S. J., et. al., "The Structure of Turbulent Boundary Layers," J. Fluid Mech., 30, 741, (1967).

26. Laufer, J., "The Structure of Turbulence in Fully Developed Pipe Flow," NACA Report 1174, (1954).

27. Logan, S. E., "A Modest Laser Doppler Instrument for Laboratory Motion Measurements," AIAA 20th Annual Region VI Student Conference, California State Polytechnic College, San Luis Obispo, (1970).

28. Logan, S. E., "A Laser Velocimeter for Reynolds Stress and Other Turbulence Measurements," AIAA J., 10, (to appear June or July, 1972).

29. Logan, S. E., "Laser Velocimeter Measurement of Reynolds Stress and Turbulence in Dilute Polymer Solutions," AIAA J., 10, (to appear June or July, 1972).

30. Lumley, J. L., "Drag Reduction by Additives," Annual Review of Fluid Mechanics, 1, 367, (1969).

31. Lumley, J. L., George, W. K., and Kobashi, Y., "The Influence of Ambiguity and Noise on the Measurement of Turbulent Spectra by Doppler Scattering," Proceedings, Symposium on Turbulent Measurements in Liquids, Rolla, Missouri, (September, 1969)

32. Metzner, A. B., and Park, M. G., "Turbulent Flow Characteristics of Viscoelastic Fluids," J. Fluid Mech., 20, 291, (1964).

33. Moody, L. F., "Friction Factors for Pipe Flow," Trans. ASME, 66, No. 8, 671, (1944).

REFERENCES (cont.)

34. Nikuradse, J., "Untersuchungen über turbulente Strömung in nicht kreisförmigen Rohren, " Ingenieur-Archiv, Julius Springer, Berlin, Germany, 1, 306, (1930).

35. Paterson, R. W., "Turbulent Flow Drag Reduction and Degradation with Dilute Polymer Solutions," PhD thesis, Div. of Eng. and Appl. Sci., Harvard U., (1969).

36. Penner, S. S., "Use of Lasers for Local Measurements of Velocity Components, Species Densities and Temperatures," AIAA 6th Aerodynamic Testing Conference, Albuquerque, New Mexico, AIAA Paper No. 71-283, (1971).

37. Pfenninger, W., "A Hypothesis of the Reduction of the Turbulent Friction Drag in Fluid Flows by Means of Additives, Etc.," 4th Winter Meeting of the Society of Rheology, (1967).

38. Phillips, O. M., "The Maintenance of Reynolds Stress in Turbulent Shear Flow," J. Fluid Mech., 27, 131, (1967).

39. Prandtl, L. "Über die ausgebildete Turbulenz," Proceedings, 2nd Internatl. Conf. for Applied Mechanics, Zurich, 62, (1927).

40. Raman, C. V., and Nath, N. S. N., "The Diffraction of Light by Sound Waves of High Frequency, Pt. II," Proc. Indian Acad. Sci., 2A, 413, (1935).

41. Rudd, M. J., "A New Theoretical Model for the Laser Dopplermeter, " Journal of Scientific Instruments (E) Series 2, 2, 55, (1969).

42. Rudd, M. J., "Measurements Made on a Drag Reducing Solution with a Laser Velocimeter," Nature, 224, 587, (1969).

43. Rudd, M. J., "Velocity Measurements Made With a Laser Dopplermeter on the Turbulent Pipe Flow of a Dilute Polymer Solution," J. Fluid Mech., 51, 4, 673, (1972).

44. Seyer, F. A.,and Metzner, A. B., "Turbulence Phenomena in Drag Reducing Systems," AIChE Journal, 15, 3, 426, (1969).

REFERENCES (cont.)

45. Spangler, J. G., Viscous Drag Reduction, (ed. C. S. Wells), Plenum Press, pp. 131-358, (1969).

46. Stevenson, W. H., "Optical Frequency Shifting by Means of a Rotating Diffraction Grating," Applied Optics, 9, 649, (1970).

47. Toms, B. A., "Some Observations on the Flow of Linear Polymer Solutions Through Straight Tubes at Large Reynolds Numbers," Proc. of First Internat. Rheol. Cong., Holland, II, 135, (1948).

48. Tracy, H. J., "Turbulent Flow in a Three Dimensional Channel," Journal of Hydraulics Division, Proc. of the American Society of Civil Engineers, HY 6, 4530,(1965).

49. Tulin, M. P., "Hydrodynamic Aspects of Macromolecular Solutions," Sixth Symposium on Naval Hydrodynamics, Washington, D.C., (1966).

50. Virk, P. S., et. al., "The Toms Phenomenon; Turbulent Pipe Flow of Dilute Polymer Solutions," J. Fluid Mech. 30, 305, (1967).

51. Walsh, M., "On the Turbulent Flow of Dilute Polymer Solutions," PhD thesis, Dept. of Aero. Eng., California Institute of Technology, (1967).

52. Wang, C. P., "New Model for Laser Doppler Velocity Measurement on Turbulent Flow," Applied Physics Letters, 18, No. 11, 522, (1971).

53. Wells, C. S., Jr., and Spangler, J. G., "Injection of a Drag-Reducing Fluid into Turbulent Pipe Flow of a Newtonian Fluid," Physics of Fluids, 10, No. 9, 1890, (1967).

54. Yeh, Y., and Cummins, H. Z., "Localized Fluid Flow Measurements with an He-Ne Laser Spectrometer," Applied Physics Letters, 4, 176, (1964).

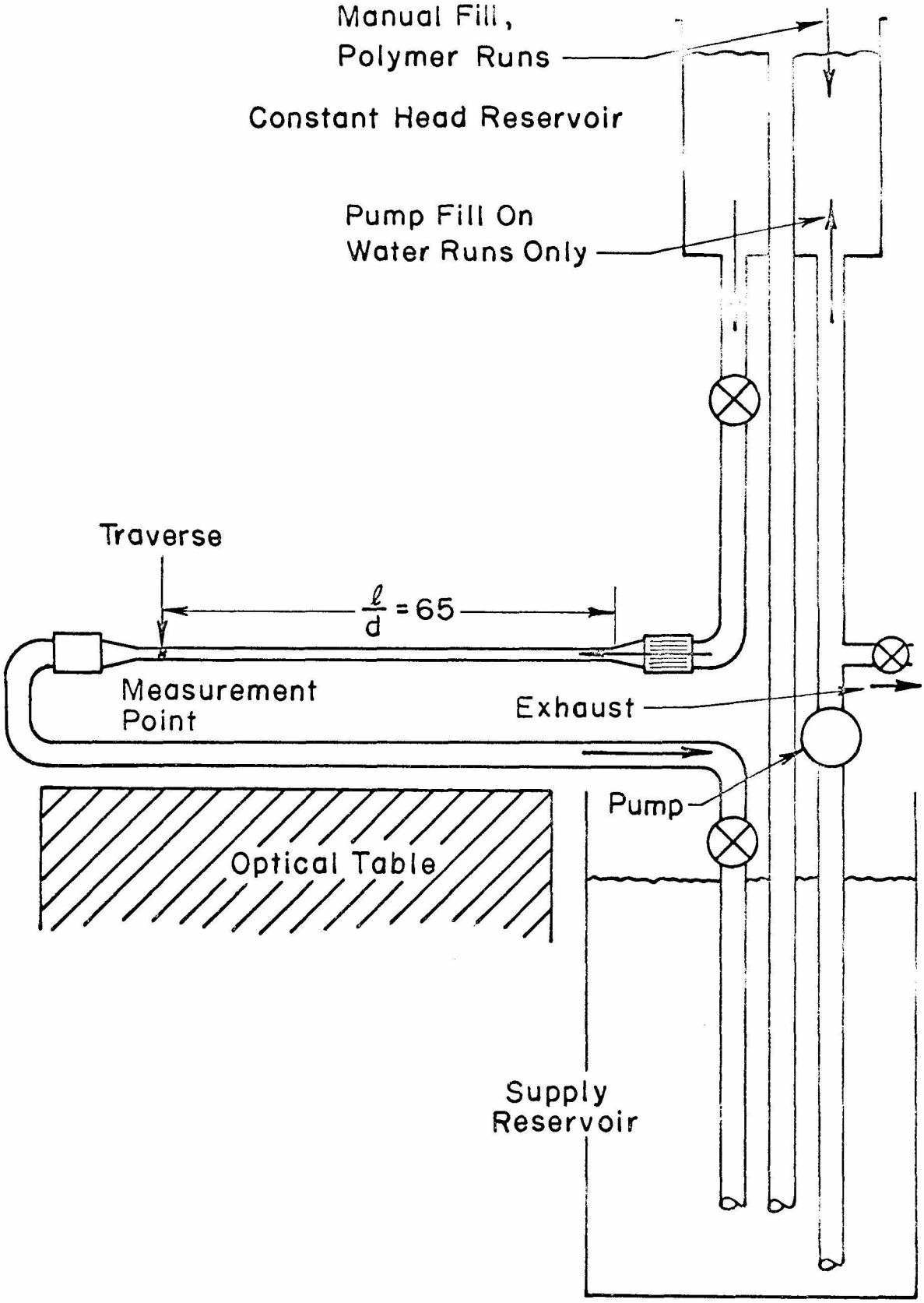

Figure 1. Flow Apparatus

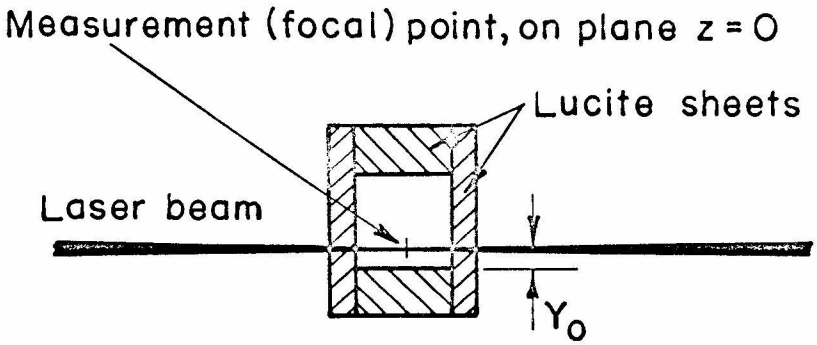

Tube Cross Section, Full Scale

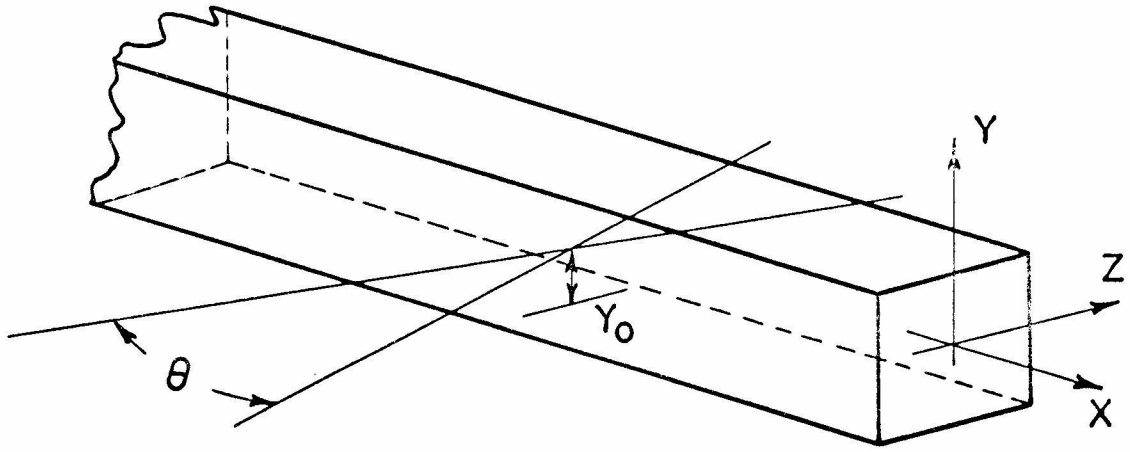

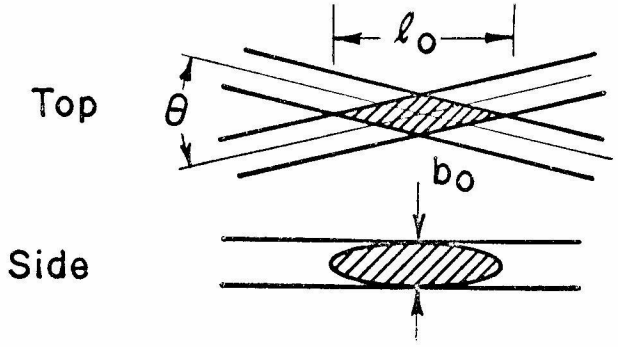

Focal Volume Schematic

Figure 2. Optical Considerations in Square Pipe Selection

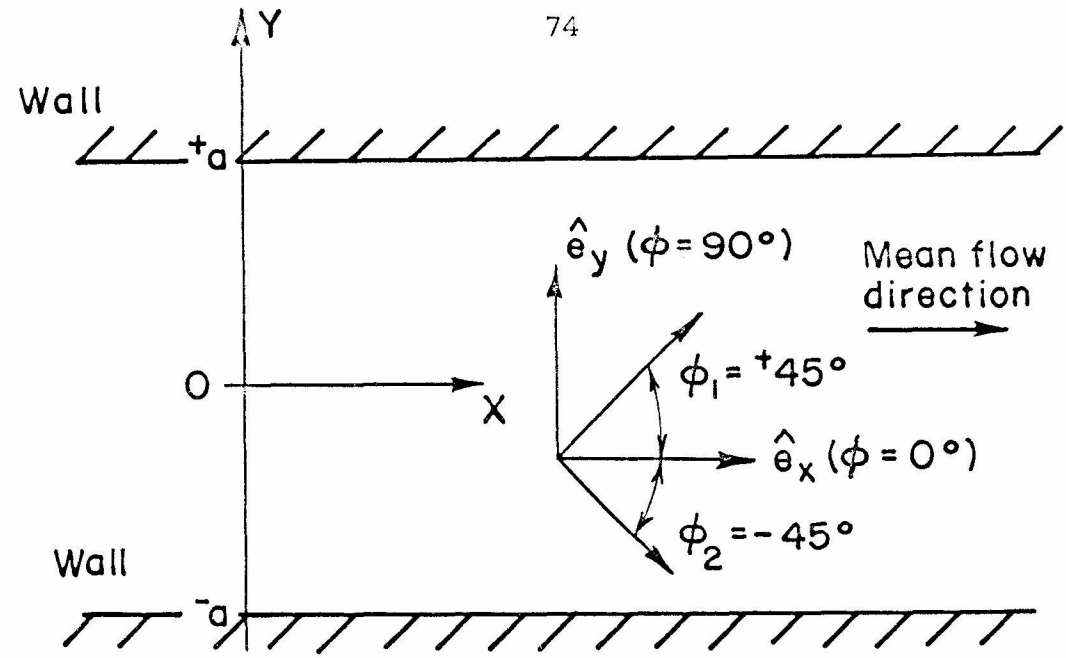

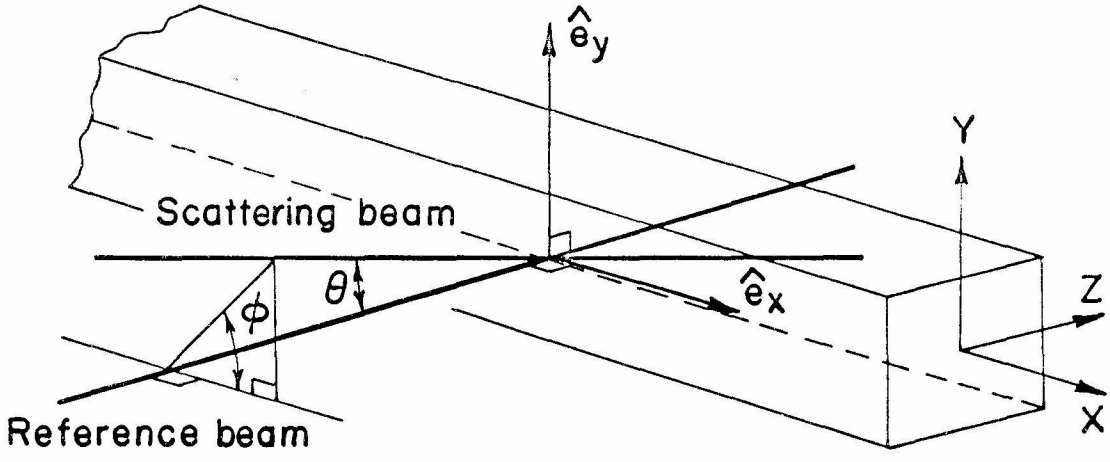

Figure 3. Definition of Angles Used in Pipe Flow Measurements

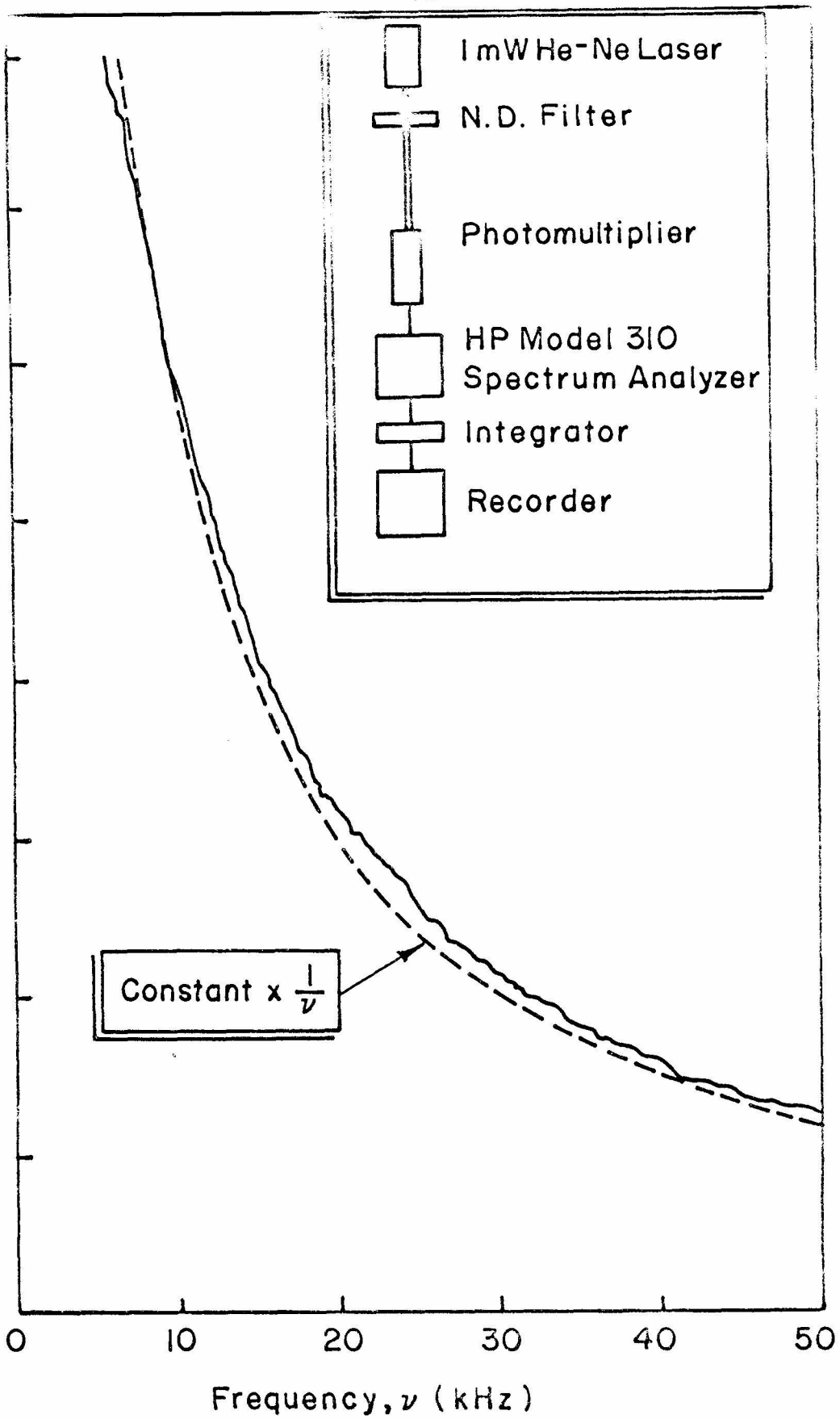

Figure 4. Low Frequency Laser Noise

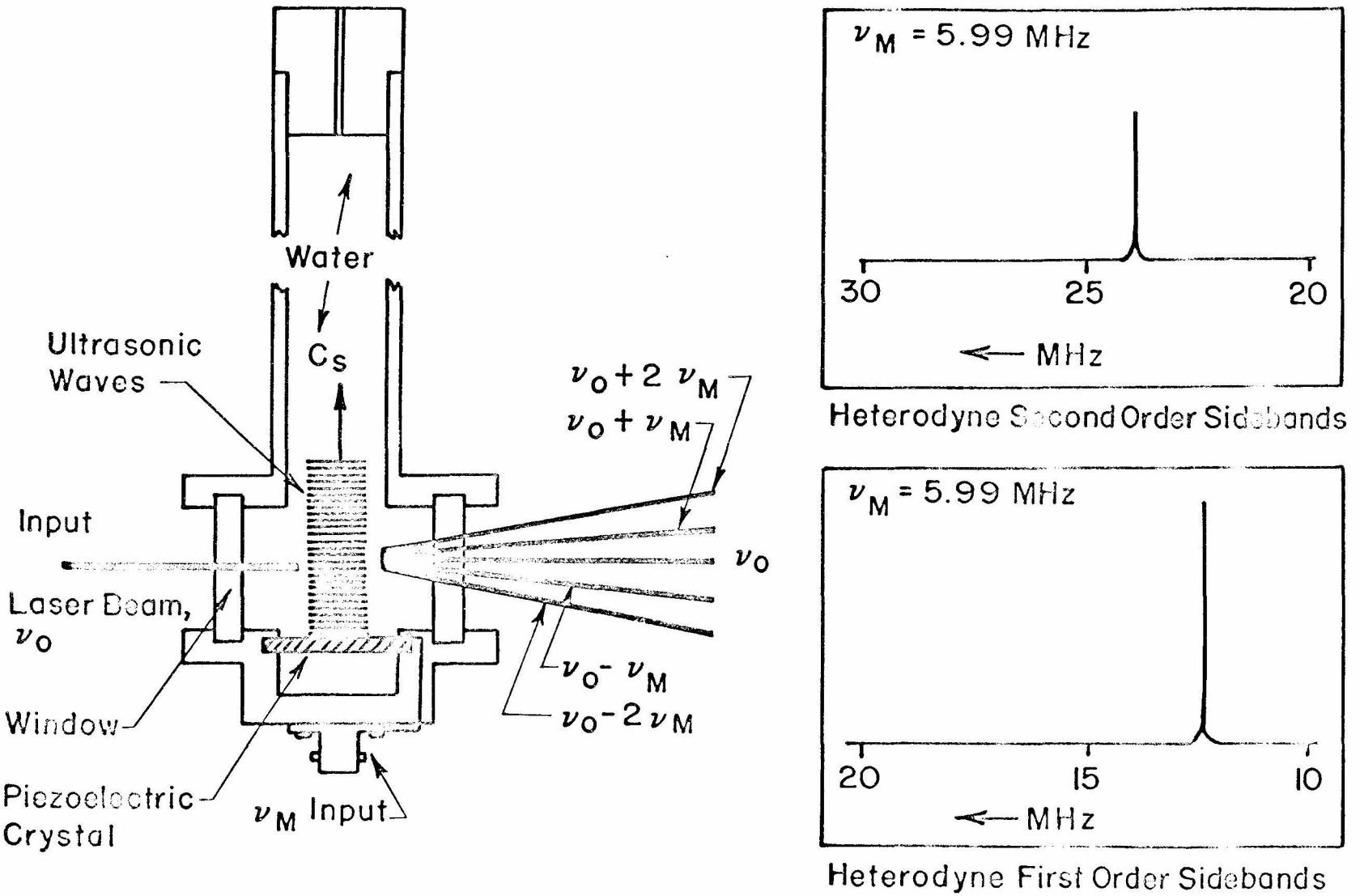

Figure 5. Frequency Modulation by Diffraction From Ultrasonic Waves in Water

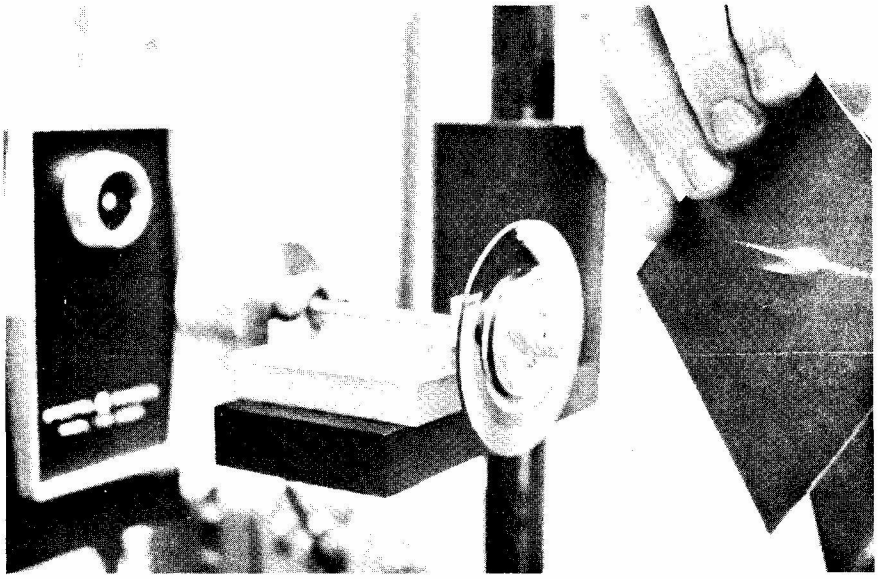

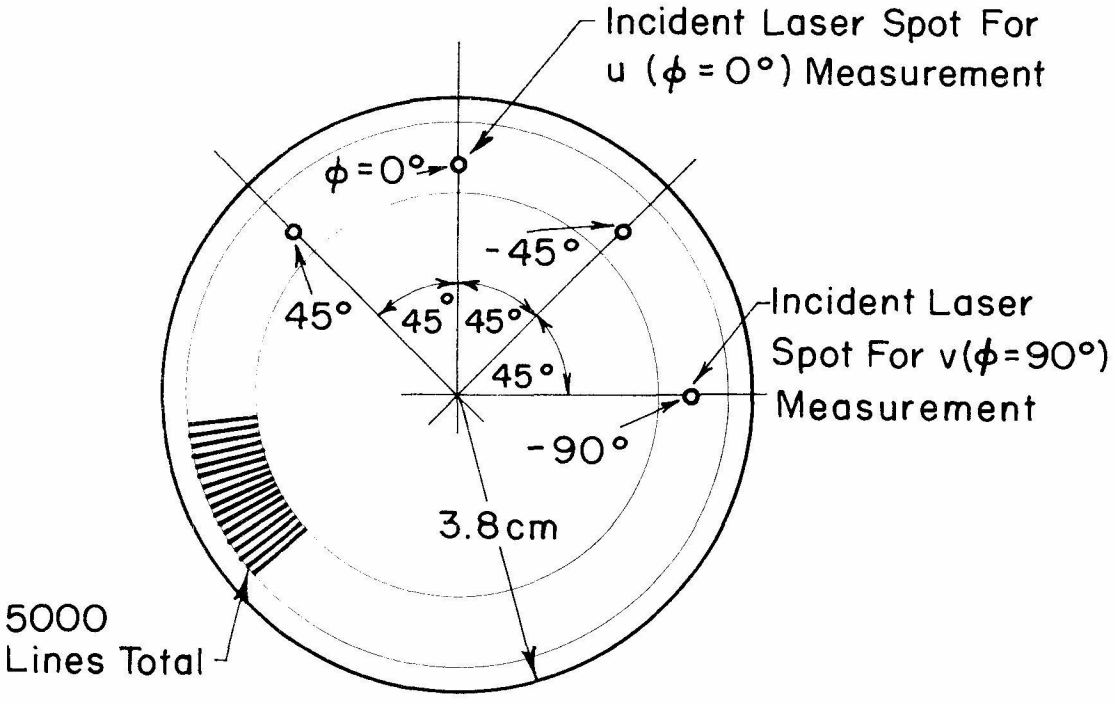

FIG. 6 THE RADIAL DIFFRACTION GRATING

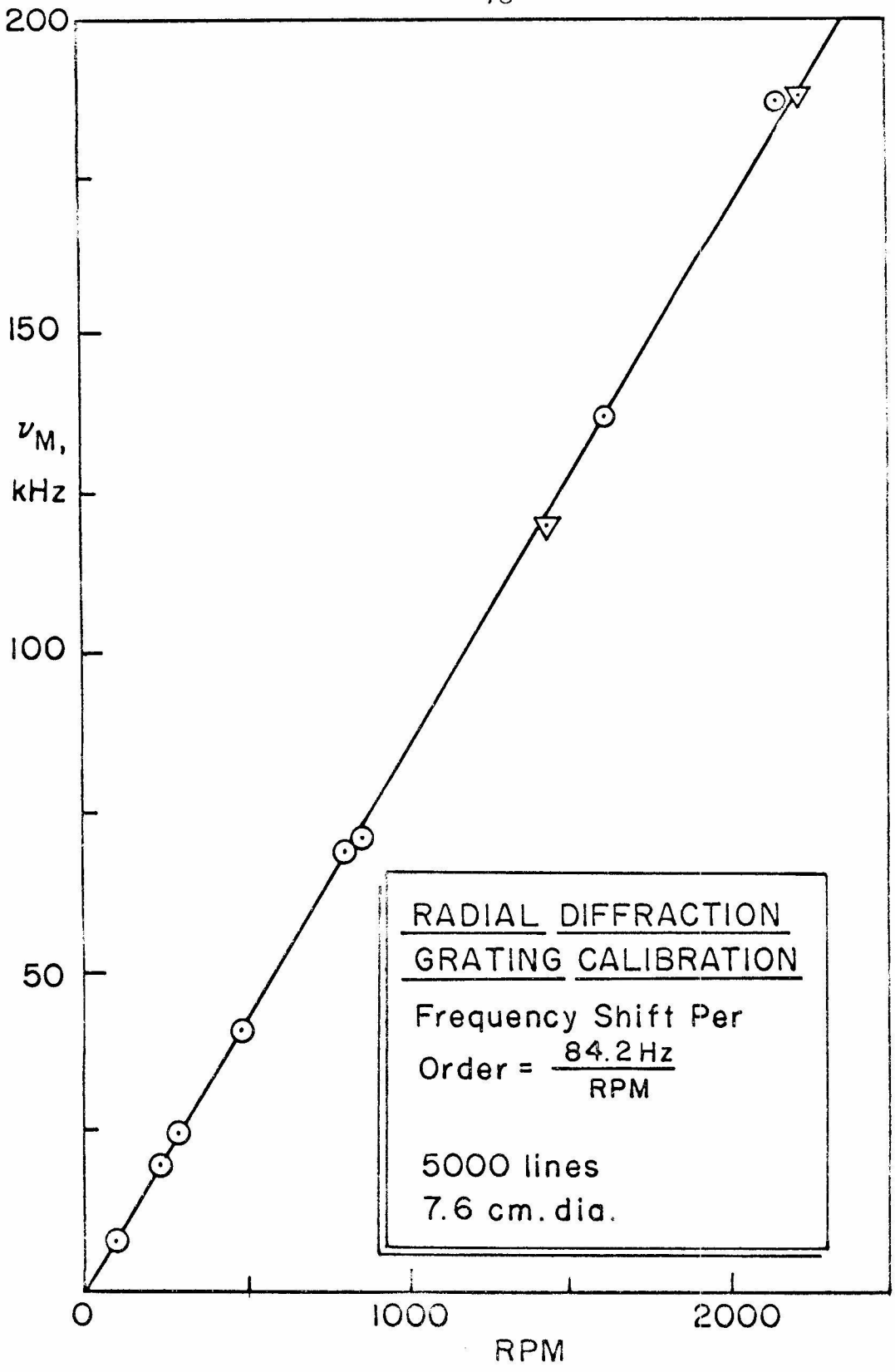

Figure 7. Radial Diffraction Grating Calibration

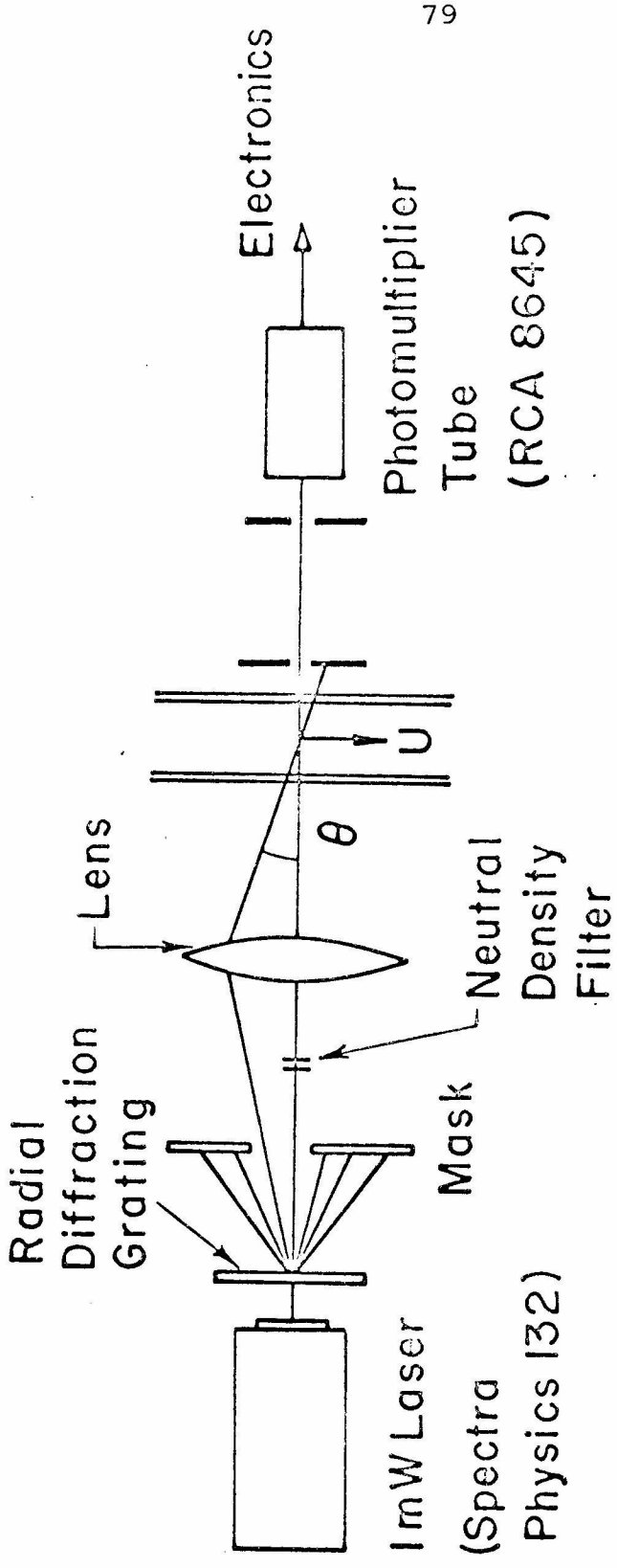

Figure 8. Laser Velocimeter Schematic

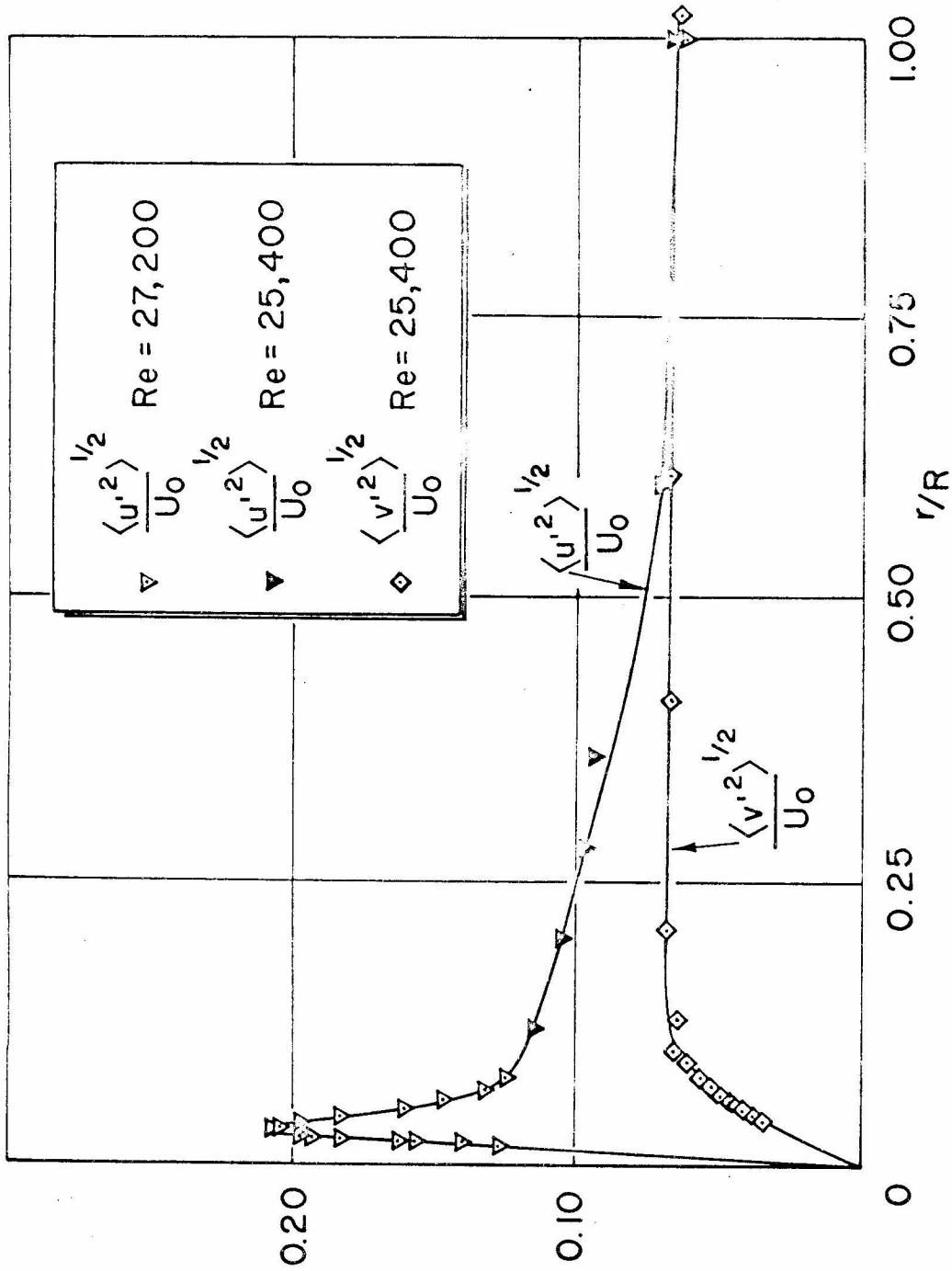

Figure 9. Axial and Radial Turbulence Intensities Across ½ Inch Square Pipe, Water.

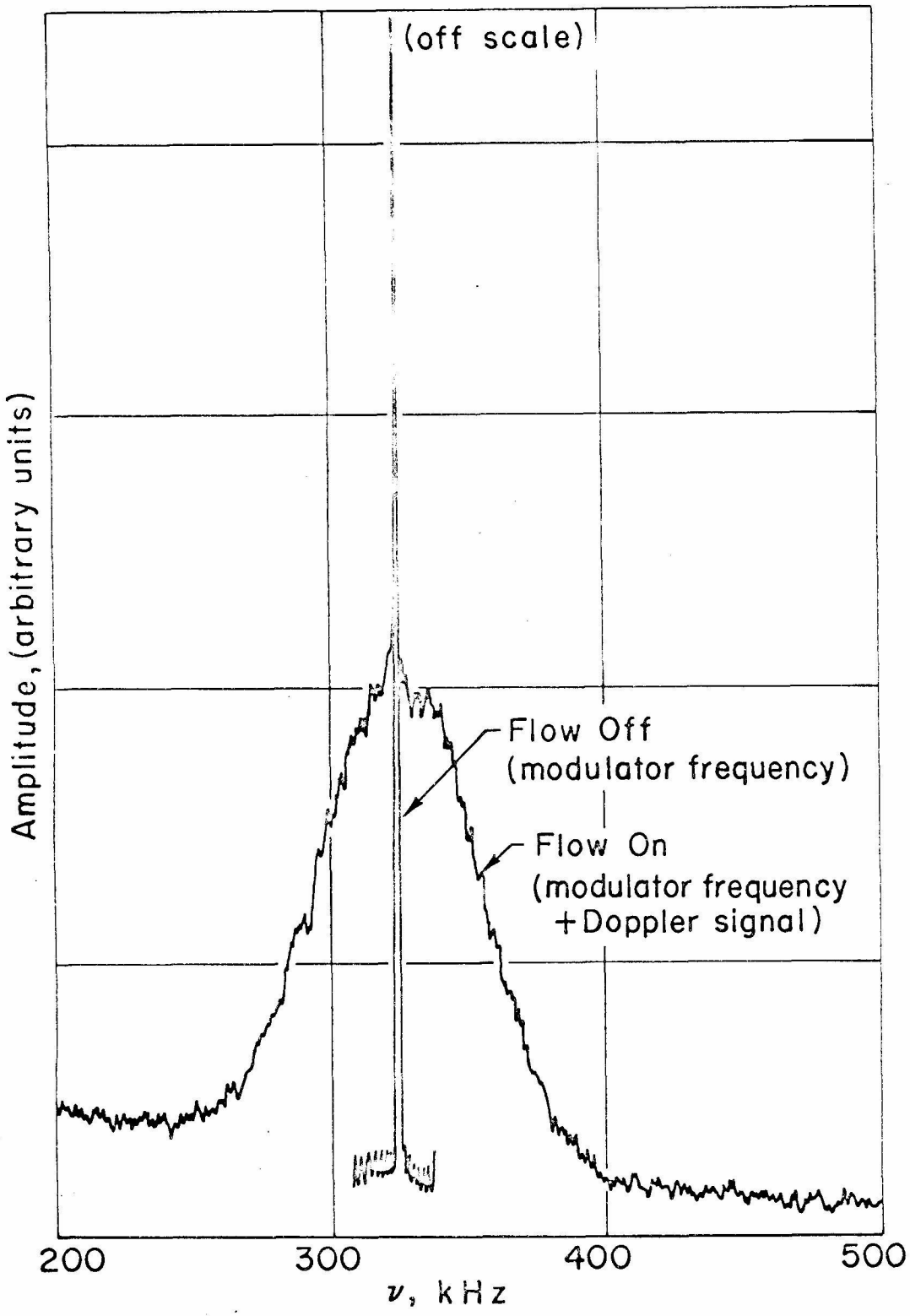

Figure 10. Typical Radial Turbulence Signal

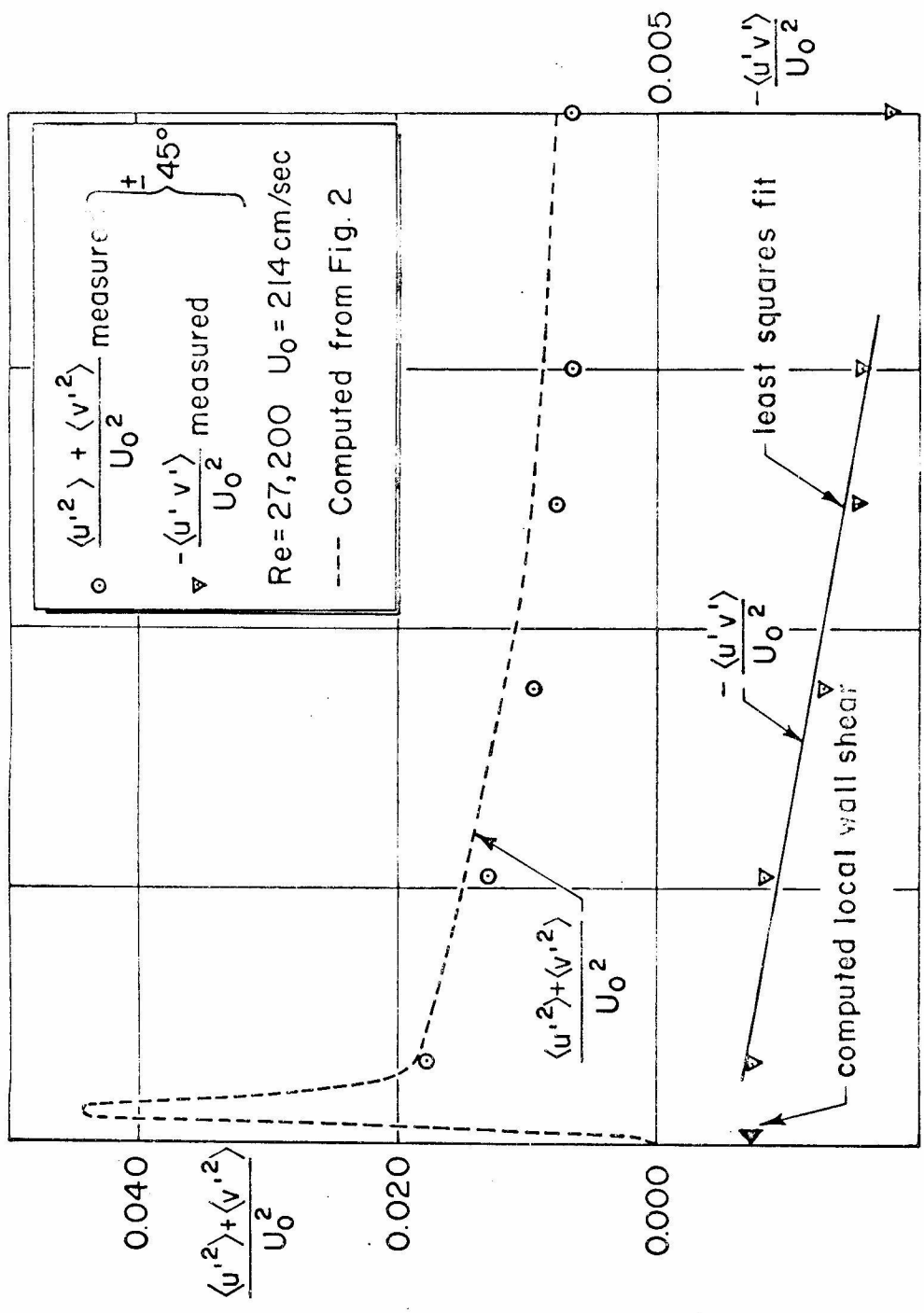

Figure 11. Reynolds Stress and Turbulent Energy Across Pipe, Water

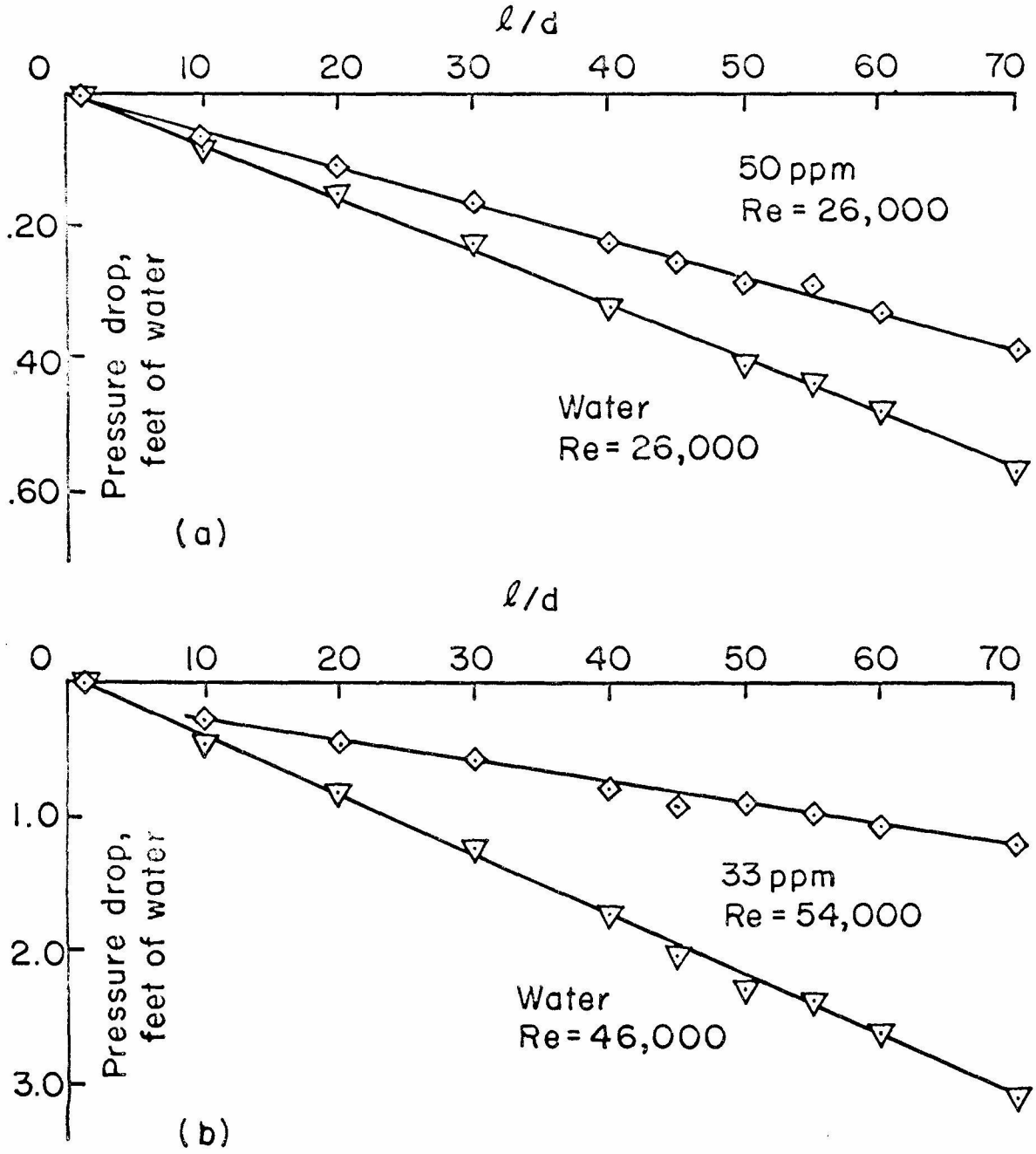

Figure 12. Representative Pressure Gradients For Water and Polymer Pipe Flow at Two Reynolds Numbers

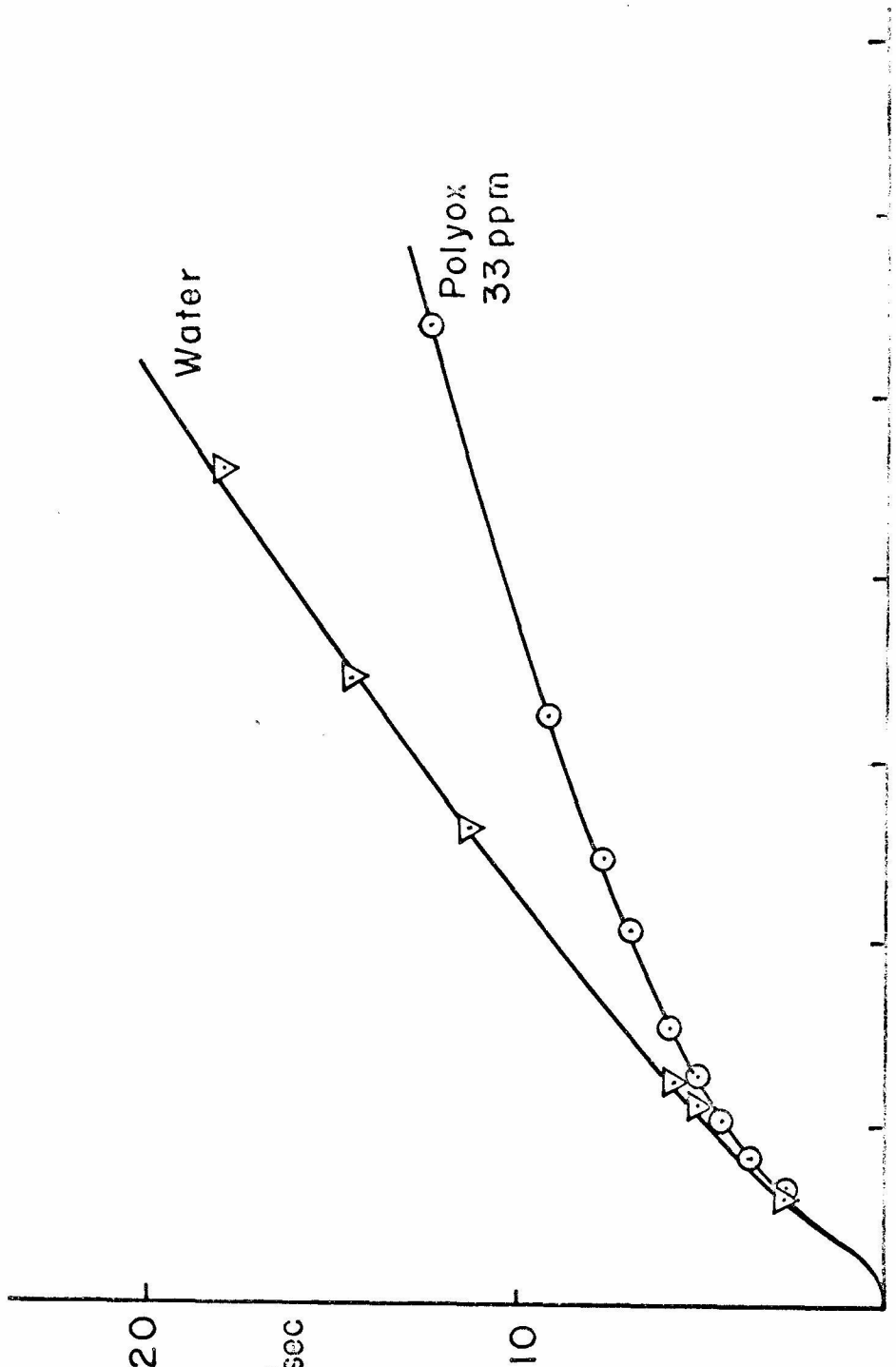

Figure 13. Shear Velocity u_τ Versus (Volume Flow) Reynolds Number For Water and Polymer Solution

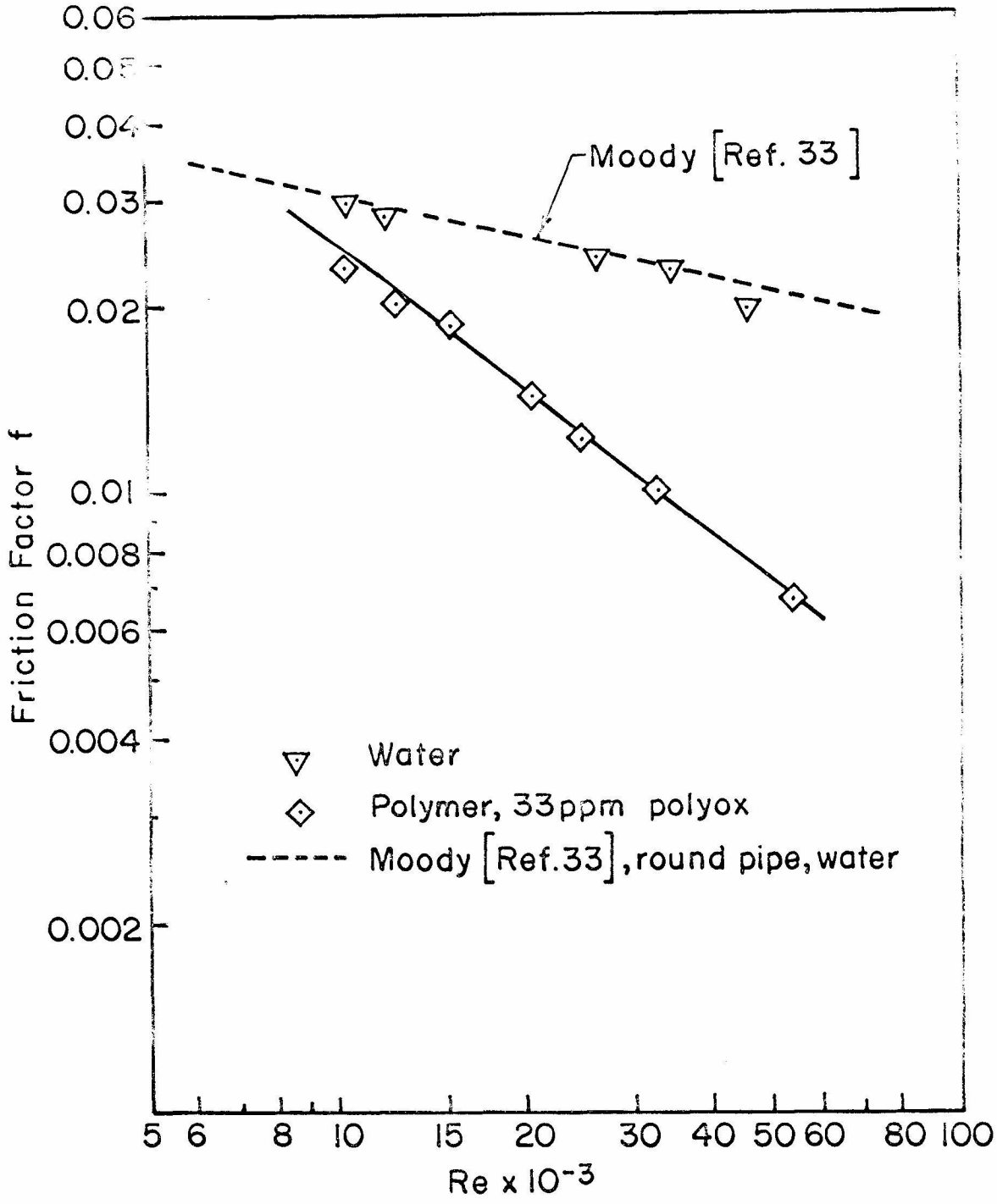

Figure 14. Friction Factor as a Function of (Volume Flow) Reynolds Number For Water and Polymer Flow in Square Pipe

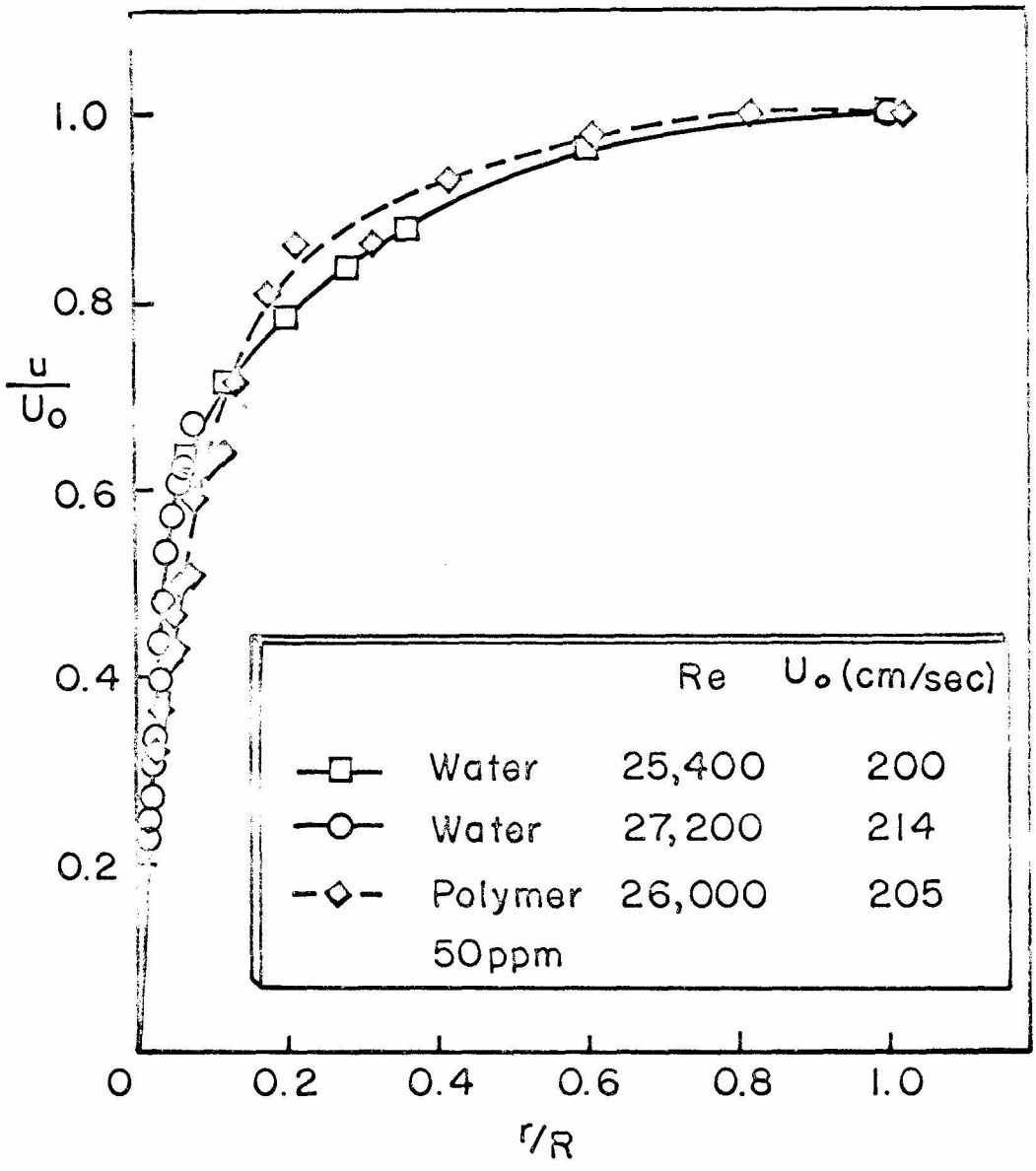

Figure 15. Mean Velocity Profiles for Water and Polymer Solution

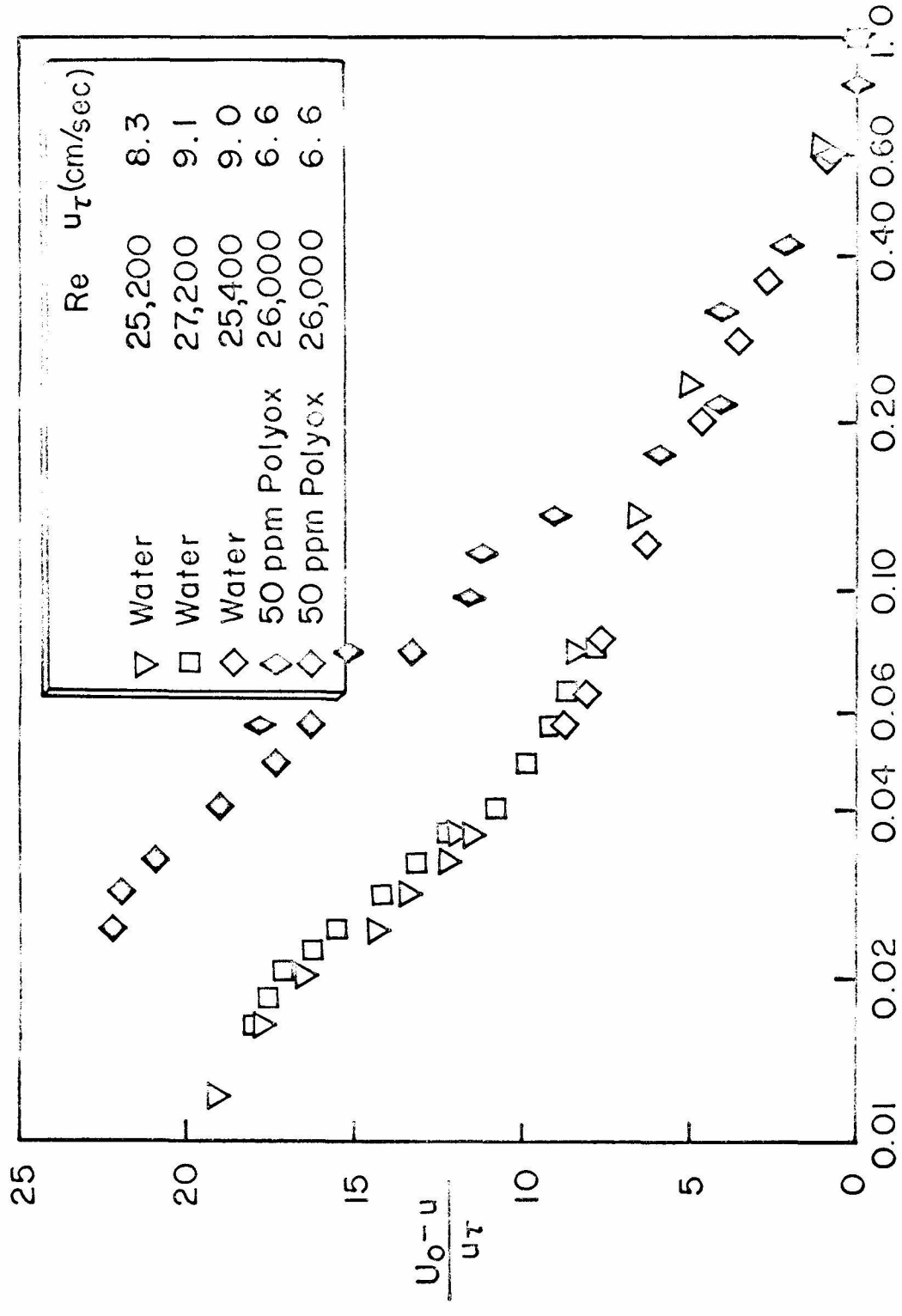

Figure 16. Velocity Defect Law for R_e = 26,000

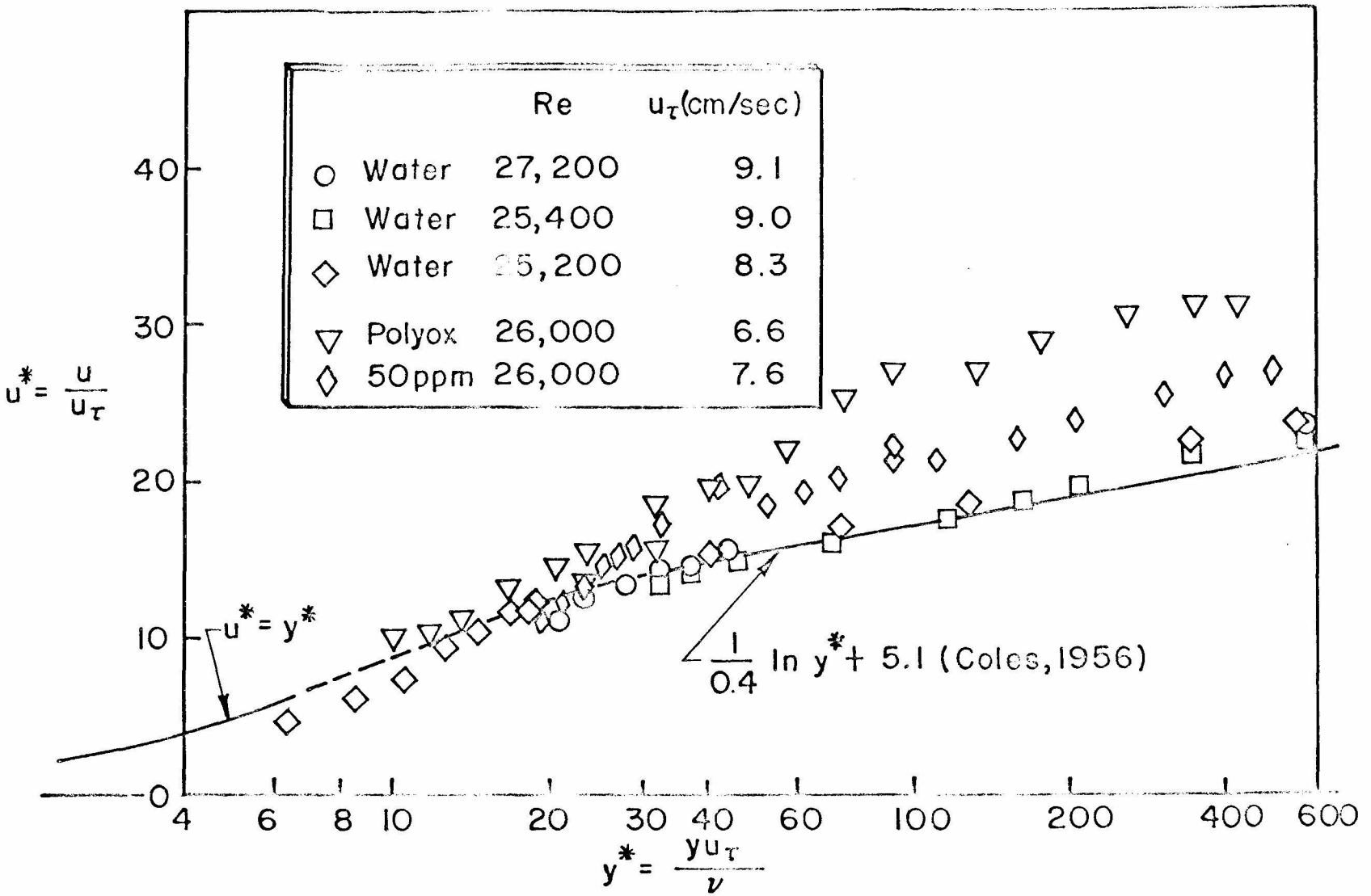

Figure 17. Velocity Profiles for Water and Polymer Compared to the Law of the Wall

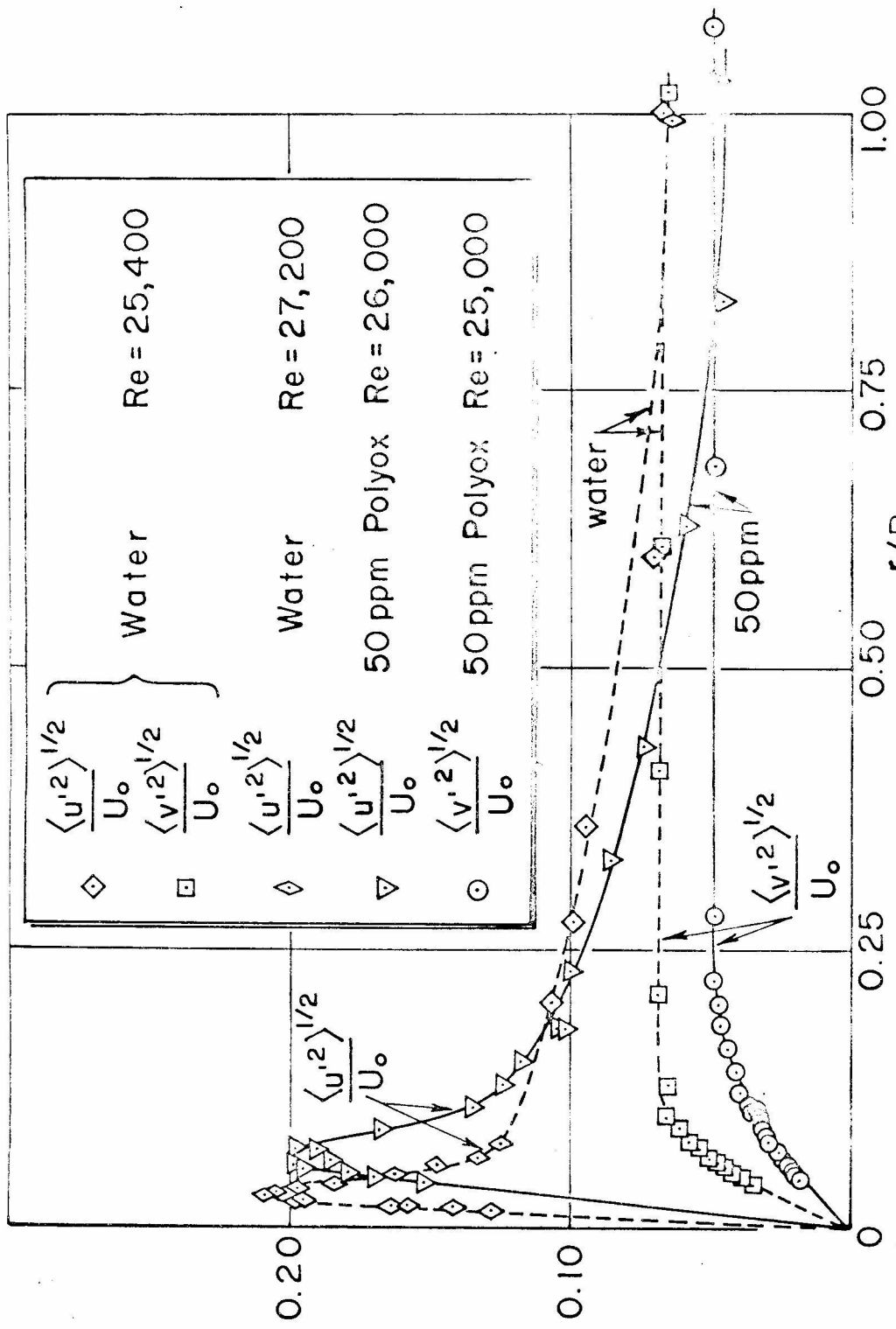

Figure 18. Axial and Transverse Turbulence Intensities Across the Pipe for Water and Polymer Solution at Re = 26,000. (From Logan (1972), Ref. 29)

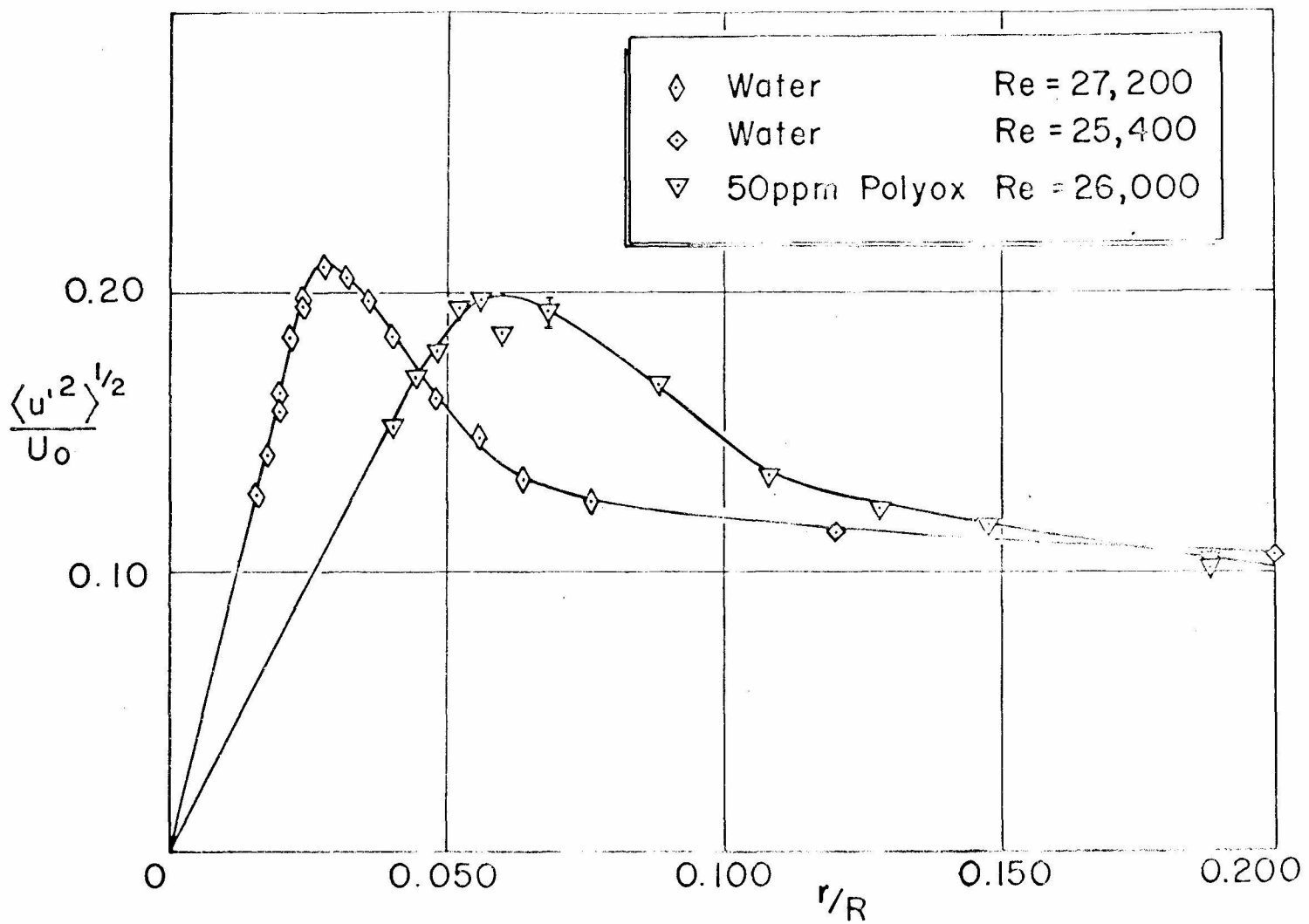

Figure 19. Axial Turbulence Intensity Near the Wall. (Logan (1972), Ref. 29)

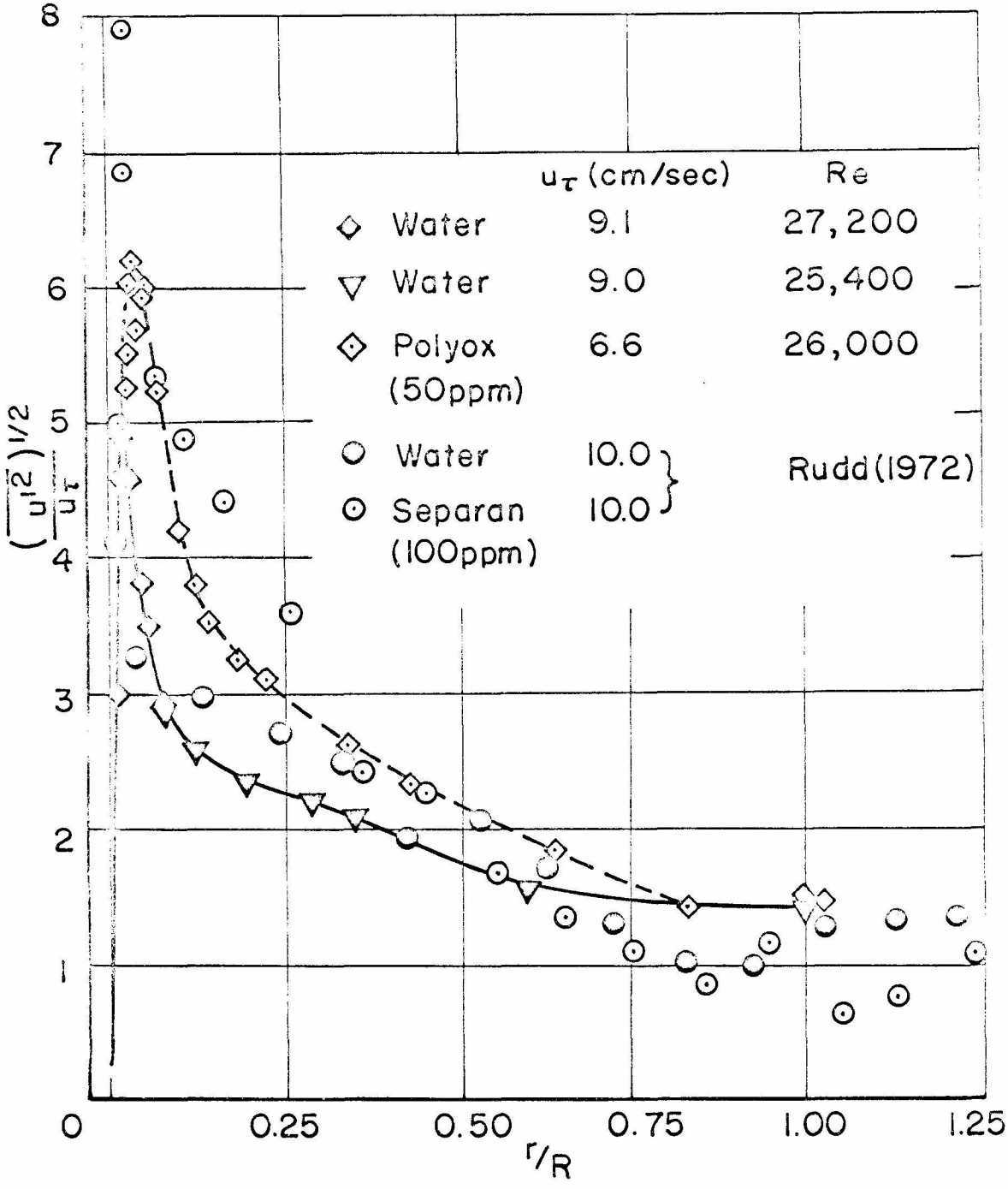

Figure 20. Comparison of Axial Intensity Across Pipe With Rudd (1972)

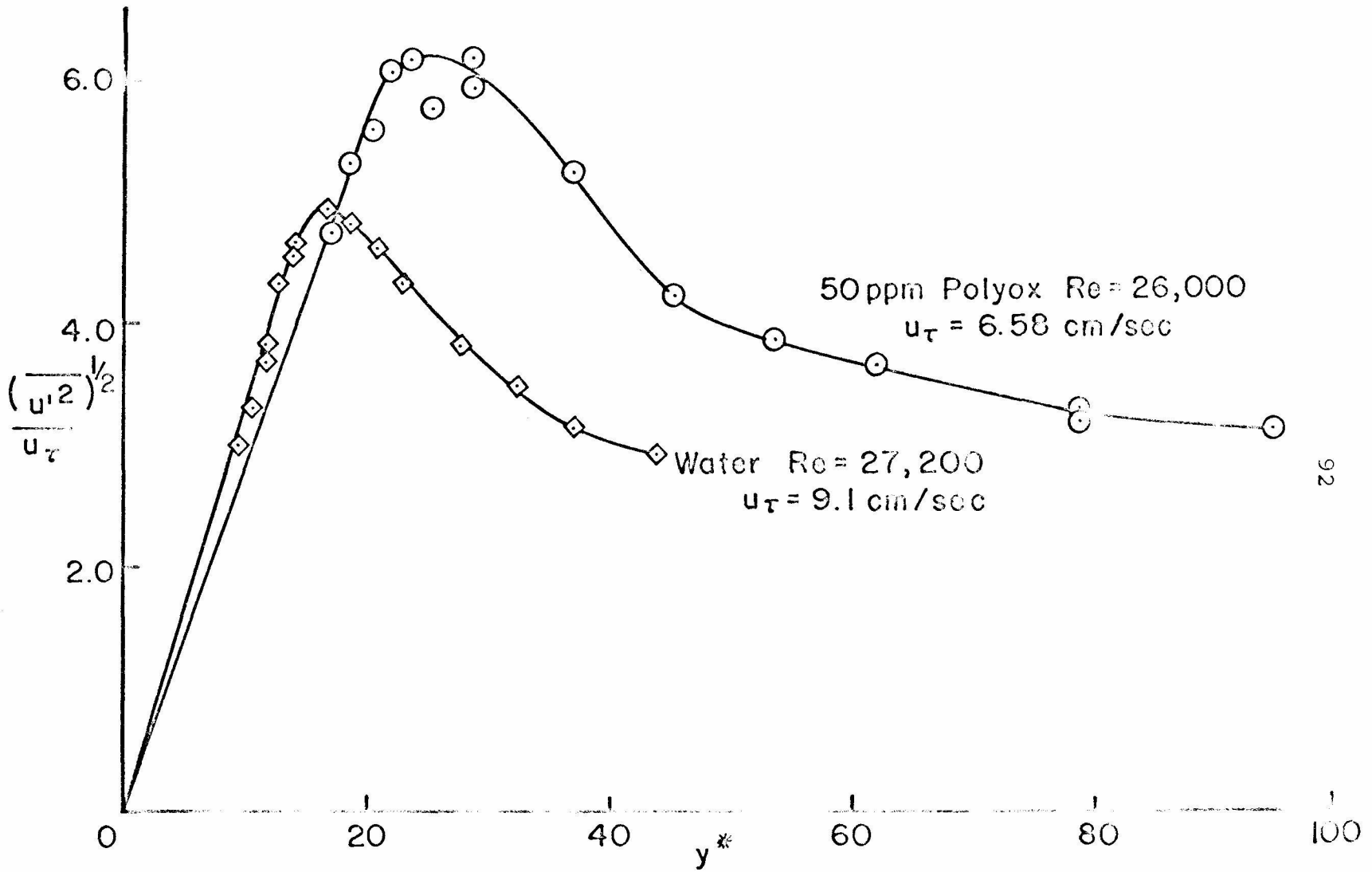

Figure 21. Axial Turbulence Intensity Near the Wall Normalized With u_τ

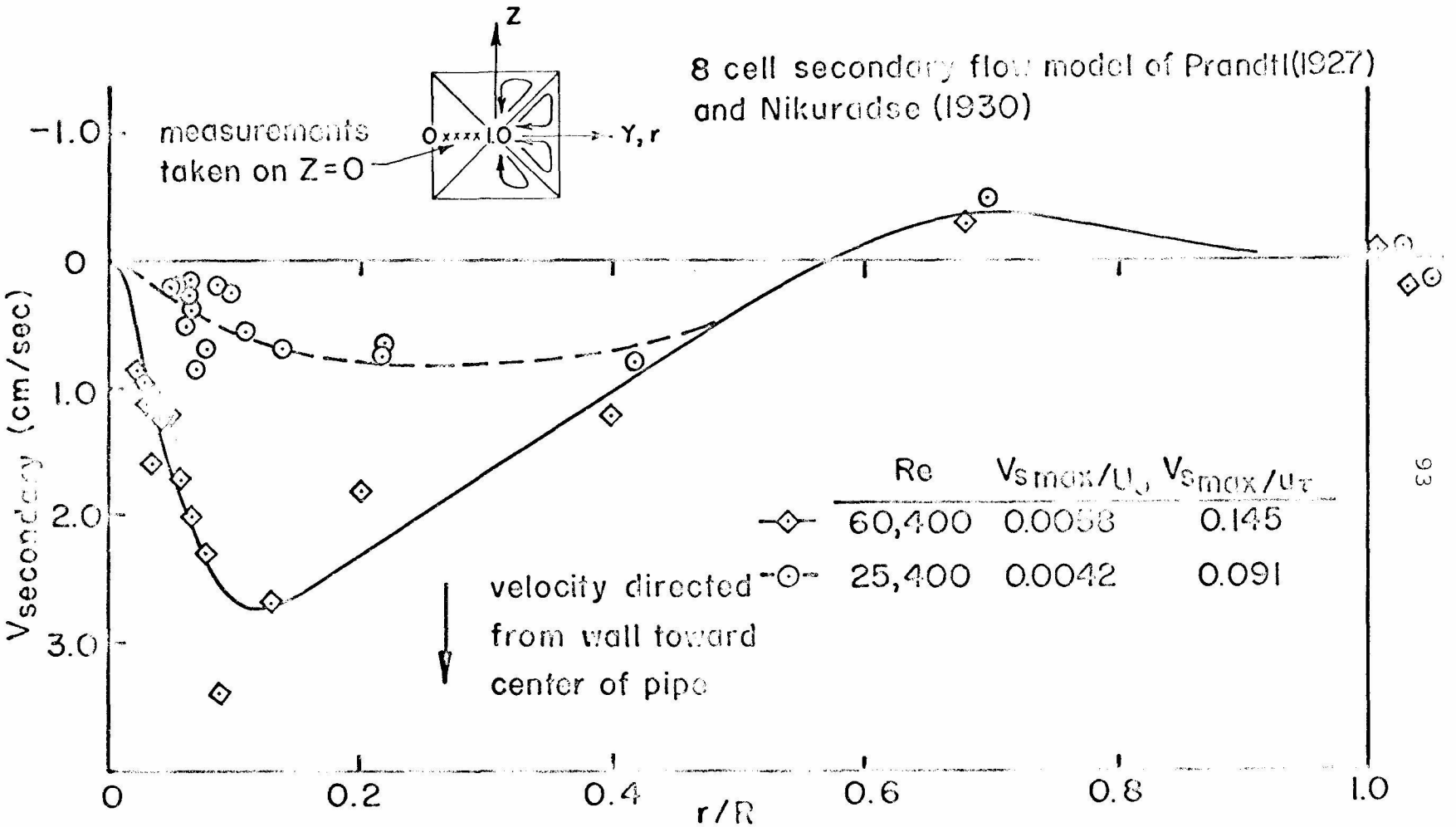

Figure 22. Radial (Secondary) Flow in the Square Pipe For Water

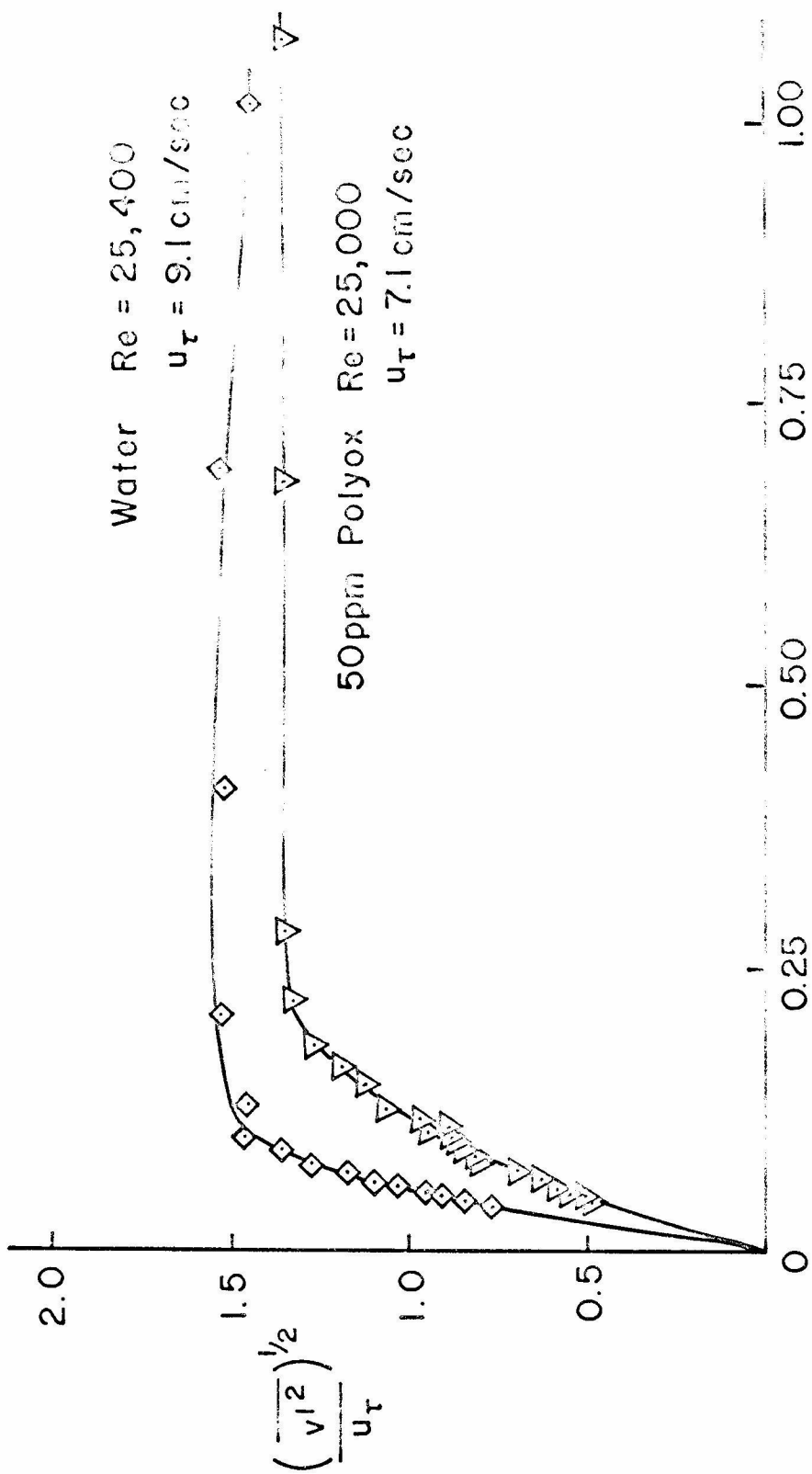

Figure 23. Radial Turbulence Intensity Across the Pipe

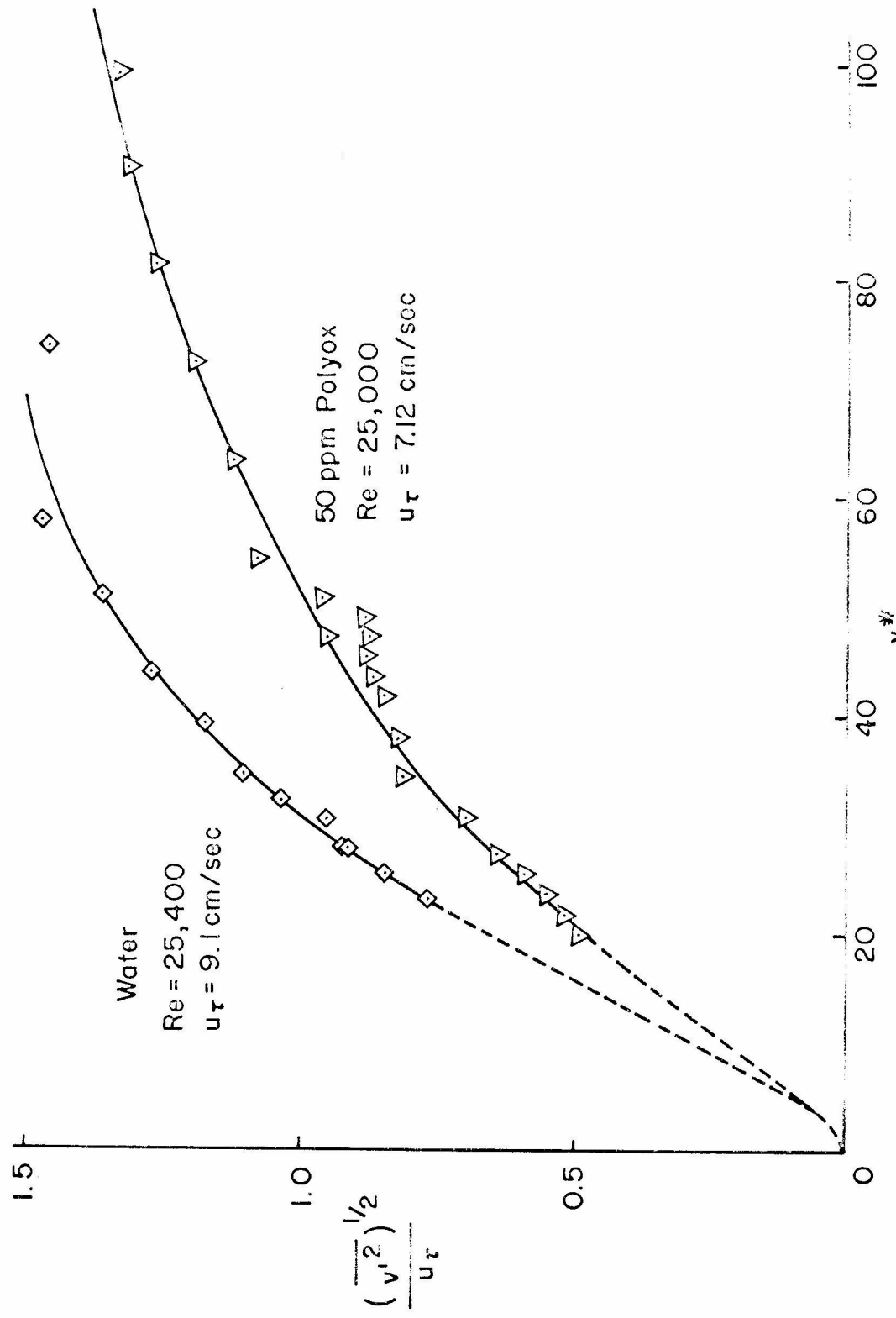

Figure 24. Radial Turbulence Intensity Near the Wall

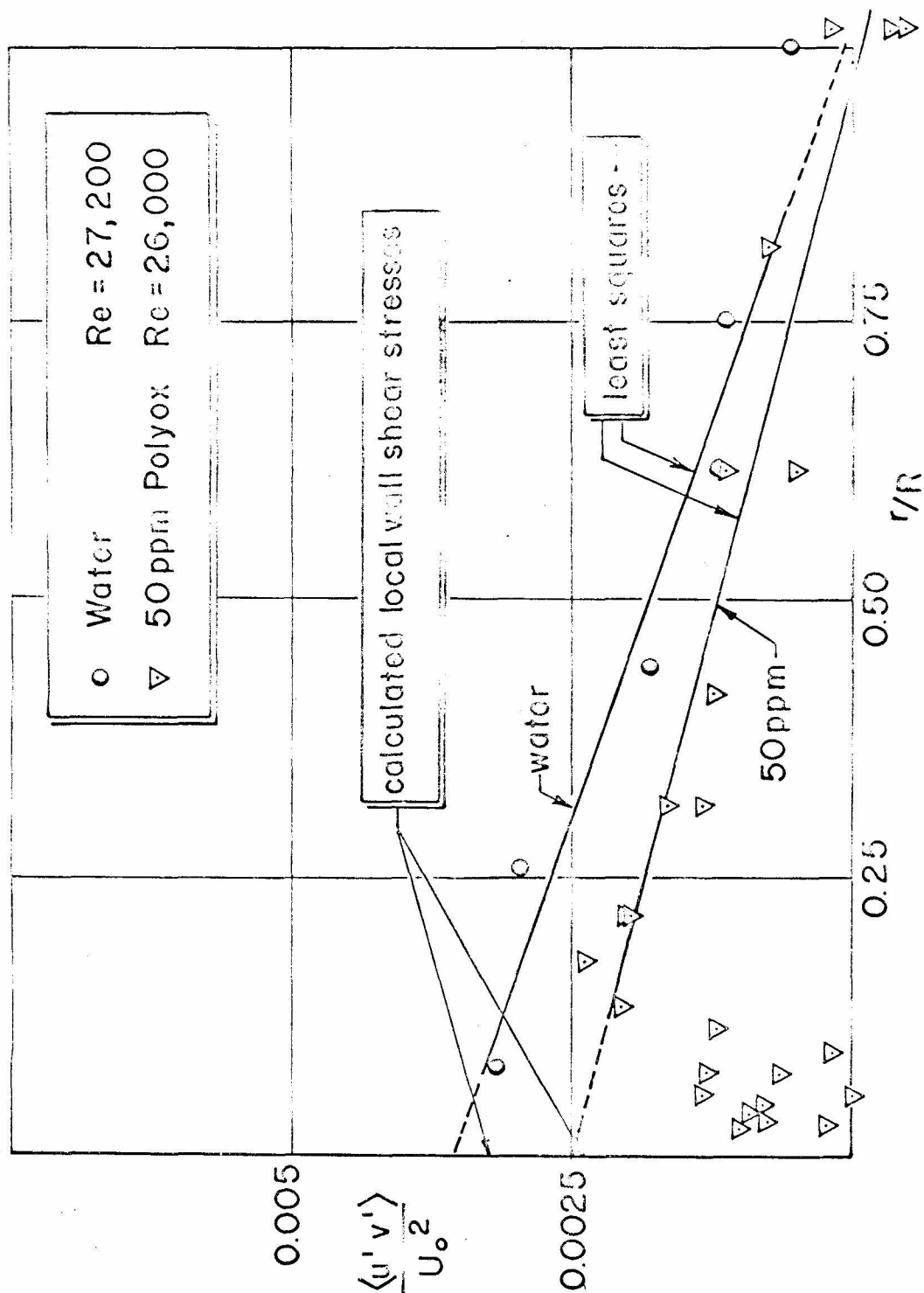

Figure 25. Reynolds Stress for Water and Polymer at Re = 26,000

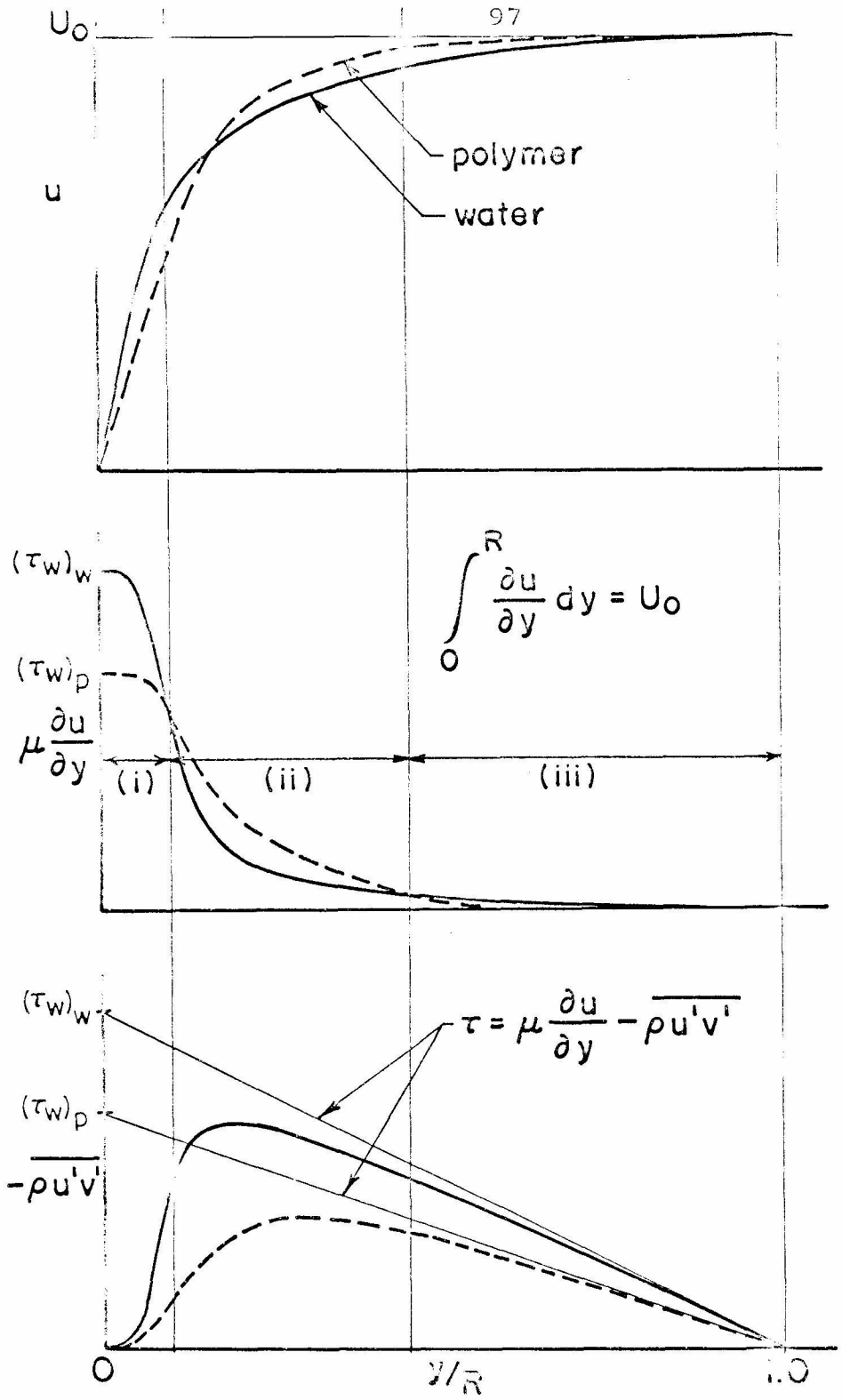

Figure 26. Schematic Representation of Relationship Between Observed Reynolds Stress Distribution and Velocity Profile in Polymer Solution

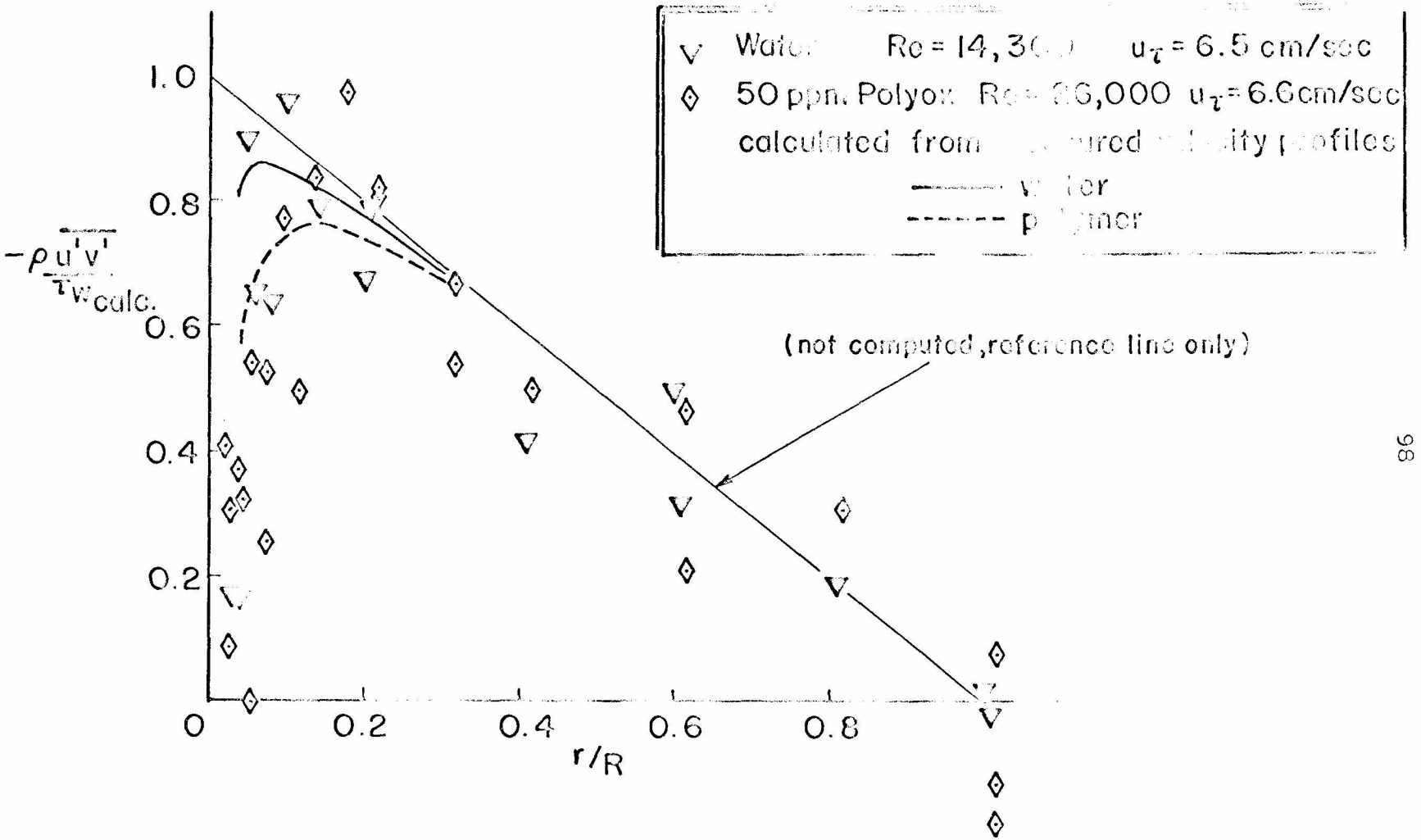

Figure 27. Comparison of Normalized Reynolds Stress for Water and Polymer at the Same Average Wall Shear, u_τ = 6.6 cm/sec